Machine Learning-Based Sedigraph Reconstruction for Enhanced Sediment Yield Estimation in the Upper Blue Nile Basin

Kindie Bitew Worku[1,2], Fasikaw A. Zimale[1], Till Francke[2], Morteza Zargar[2] and Axel Bronstert[2]

[1]Faculty of Civil and Water Resources Engineering, Bahir Dar Institute of Technology, Bahir Dar University, Bahir Dar, P.O. Box 26, Ethiopia.
[2]Department of Hydrology and Climatology, Institute of Earth and Environmental Science, University of Potsdam, Potsdam, Germany.
Corresponding author: kindiebitew@gmail.com; kindie.worku@uni-potsdam.de

ABSTRACT

Sediment-laden runoff in Ethiopia's Upper Blue Nile Basin (UBNB) threatens the ecological balance of Lake Tana and the operational efficiency of the Grand Ethiopian Renaissance Dam (GERD), a critical hydropower infrastructure. High sediment loads, driven by intense monsoon rainfall and erodible soils, exacerbate erosion and sedimentation, affecting water quality and the longevity of infrastructure across the basin. Limited data availability and complex hydrological dynamics hinder accurate measurement and modeling of sediment yields. This study reconstructs 1990–2020 sedigraphs for Gilgel Abay (1,664 km²) and Gumara (1,394 km²) watersheds using machine learning (Gradient Boosting (GB), Random Forest (RF), Quantile Random Forest (QRF)) and traditional sediment rating curves (SRCs), utilizing intermittent Suspended Sediment Concentration (SSC) measurements and continuous predictors (discharge, rainfall, temperature, and evapotranspiration). QRF provided the highest accuracy (R^2 = 0.73–0.75), capturing non-linear sediment dynamics and quantifying uncertainty via its 0.05–0.95 conditional quantile bounds. The average annual sediment yields were 30.7±7.2 t/ha/yr for the Gilgel Abay watershed and 27.5±10.74 t/ha/yr for the Gumara watershed, with 95–96% occurring during the wet season (June–October). Despite challenges from incomplete datasets due to instrument malfunctions and logistical constraints during extreme rainy events, QRF's robust predictions inform the application of targeted erosion control strategies, such as reforestation and urban runoff mitigation, to enhance sustainable management of the UBNB. This approach bridges the reconstruction of sediment concentration measurements with data gaps while improving hydrological process understanding, offering a scalable framework for sediment management in monsoon-dominated basins.

Keywords: Machine Learning, Sedigraph Reconstruction, Monsoon Hydrology, Quantile Random Forest, Land Use Change, Upper Blue Nile Basin

1. INTRODUCTION

Sediment transport is a pivotal process governing riverine ecosystem function, water quality, and infrastructure resilience, with far-reaching implications for global biogeochemical cycles (Walling and Fang, 2003; Syvitski *et al.*, 2005). Recent advances in hydrological science have highlighted how climate-driven changes are intensifying erosion and altering sediment delivery regimes worldwide, particularly through amplified hydrological variability (Zhang *et al.*, 2022a). At the same time, the rapid development of machine learning techniques has transformed our ability to model complex hydrological processes and reconstruct time series in data-scarce environments (Nearing *et al.*, 2021; Worku *et al.*, 2026). In Ethiopia's UBNB, which contributes over 60% of the Nile River's flow, these dynamics sustain agriculture, hydropower, and water security for more than 200 million people across Ethiopia, Sudan, and Egypt (Conway, 2000; Bihonegn and Awoke, 2025). However, intensified monsoon-driven sediment fluxes threaten the ecological integrity of Lake Tana, Ethiopia's largest freshwater lake, and challenge the operational safety of the Grand Ethiopian Renaissance Dam (GERD), a nationally funded infrastructure project widely regarded as a cornerstone of regional energy development (Abtew and Dessu, 2019; Annys *et al.*, 2019). Transboundary impacts for economic stability and livelihoods further exacerbate these challenges (Zegeye *et al.*, 2016).

The Gilgel Abay and Gumara watersheds, primary tributaries to Lake Tana, exemplify these sediment-related pressures (Engida, 2010). Steep slopes, erodible soils (Vertisols and Andosols), and rapid land-use changes amplify sediment yields during the wet season (Haregeweyn *et al.*, 2017; Gashaw *et al.*, 2018). Accurate quantification of sediment yields is hindered by obstacles such as extreme spatio-temporal variability and persistent data scarcity (Carrivick and Tweed, 2021). Intermittent suspended sediment concentration (SSC) measurements at Gilgel Abay and Gumara stations, disrupted by logistical constraints, instrument errors, and extreme rainy events, yield disjointed records that are insufficient for capturing event-scale dynamics or establishing long-term trends (Tebebu *et al.*, 2010; Zeleke *et al.*, 2013). This data gap challenges reliable sedigraph (SSC time series) reconstruction, which is critical for erosion control, reservoir capacity planning, and adaptive water resource management (Horowitz, 2003; Francke *et al.*, 2008; Schmidt *et al.*, 2023). Traditional Sediment Rating Curves (SRCs) often fail to capture the non-linear hydro-sedimentary responses to discharge, rainfall, and land-use variability in monsoon-dominated areas (Kar and Sarkar, 2022), while statistical gap-filling methods lack robustness for the UBNB's threshold-driven sediment regimes (Asselman, 2000; Ariano and Ali, 2024).

Machine learning (ML) offers a powerful approach, utilizing sparse, multivariate datasets to model complex, non-linear datasets and quantify uncertainty (Francke *et al.*, 2008; AlDahoul *et al.*, 2022). Although process-based models and empirical relationships have been applied in the UBNB (Elsanabary and Gan, 2015; Bihonegn and Awoke, 2025), ML techniques such as Gradient Boosting (GB), Random Forest (RF), and Quantile Random Forest (QRF) were selected for their ability to model non-linear sediment-discharge relationships, handle sparse datasets, and, in QRF's case, quantify prediction uncertainties critical for monsoon-driven systems like the UBNB (Meinshausen, 2006; Zhu *et al.*, 2019).

This study develops an ML framework to reconstruct continuous 31-year (1990–2020) Sedigraphs for the Gilgel Abay and Gumara watersheds, addressing three objectives: (1) evaluate the performance of SRC, GB, RF, and QRF in reconstructing Sedigraphs and estimating sediment yields, (2) compare ML model accuracy against SRCs in capturing non-linear sediment dynamics, and (3) assess model potential to inform erosion management under evolving land use and climate pressures. By using QRF-based uncertainty quantification to provide robust sediment yield estimates with confidence intervals, this work bridges monitoring gaps in sparse datasets, enhances understanding of hydrological processes, and supports sustainable management in the geopolitically vital Nile Basin.

2. DATA AND METHODS

This study reconstructs continuous sedigraphs (time series of suspended sediment concentration, SSC) for the Gilgel Abay and Gumara watersheds in the UBNB from 1990 to 2020 to assess sediment dynamics and support the sustainable management of Lake Tana and the Grand Ethiopian Renaissance Dam (GERD). Four modeling approaches, SRC, GB, RF, and QRF, were employed to predict daily SSC, utilizing intermittent field observations with continuous hydrological predictors.

2.1 Study Area

The Gilgel Abay and Gumara watersheds, located in Ethiopia's UBNB upstream of Lake Tana in the Amhara Region, are critical contributors to the region's hydrological and sediment dynamics (Negatu *et al.*, 2022). Gilgel Abay spans 1,664 km², with elevations ranging from 1,787 m above sea level (a.s.l) at its outlet near Lake Tana to 3,528 m a.s.l. in the Choke Mountains, encompassing rugged highlands, dissected plateaus, and flatter lowlands that amplify runoff and erosion. Gumara covers 1,394 km², with elevations from 1,794 m a.s.l. to

3,704 m a.s.l., featuring steep highland areas transitioning to gentler lowlands toward Lake Tana, enhancing sediment mobilization (Fenta *et al.*, 2017). These elevation gradients, combined with the UBNB's tropical highland climate, drive intense erosive processes, particularly during the wet season, which delivers 80–90% of annual precipitation (Conway, 2000). Gauging stations for Gilgel Abay and Gumara, with ten meteorological stations (five per watershed) with watershed boundaries and station locations, are shown in Figure 1.

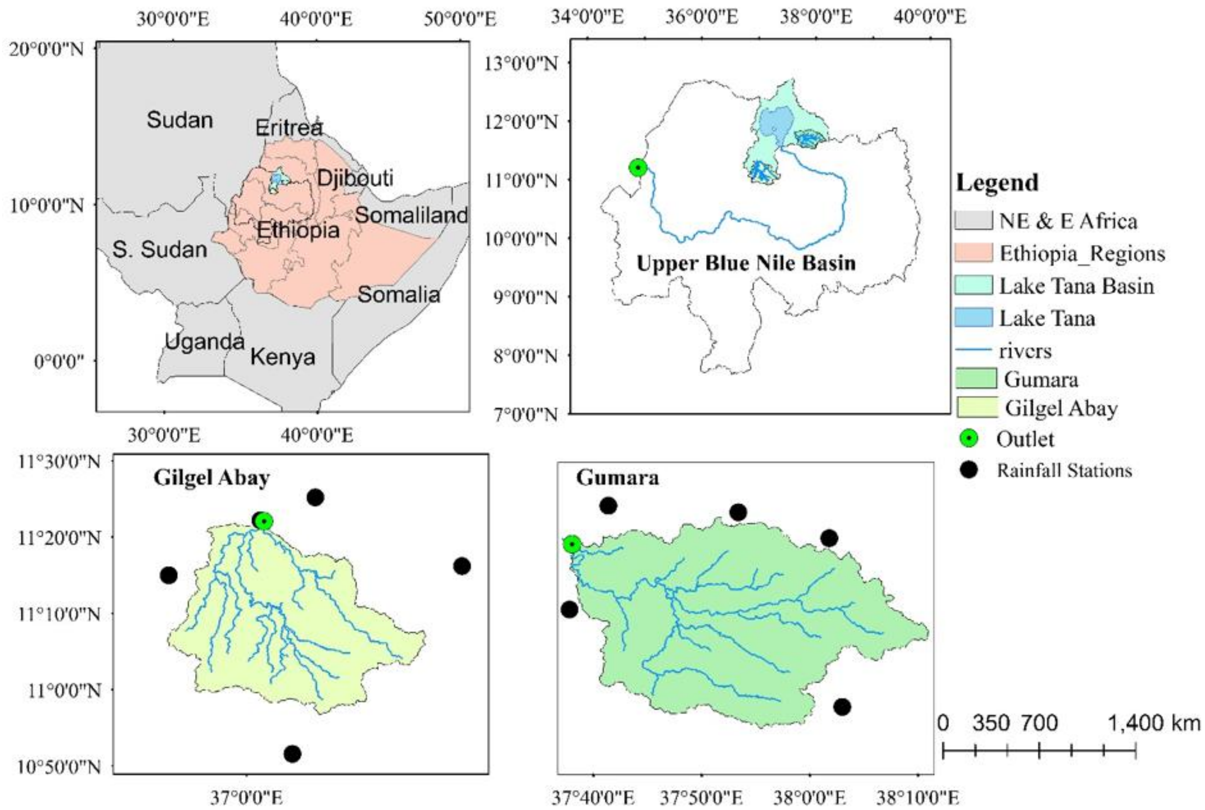

Figure 1. Location of the Gilgel Abay and Gumara watersheds within the Upper Blue Nile Basin, Ethiopia, showing river networks, rainfall stations, and outlet points.

Gilgel Abay receives an average annual rainfall of 1,861 mm and reference evapotranspiration (ETo) of 1380 mm, while Gumara experiences 1,403 mm of rainfall and 1321 mm of ETo, with 80–90% of rainfall concentrated from June to September, driving significant runoff on steep slopes and low-permeability vertisols, supplemented by minor groundwater contributions at an average temperature of 18–22°c (Teshome and Demissie, 2022). This unimodal rainfall pattern, illustrated by monthly averages of precipitation and ETo (Figure 2), sustains high runoff and sediment transport (Ayele *et al.*, 2016).

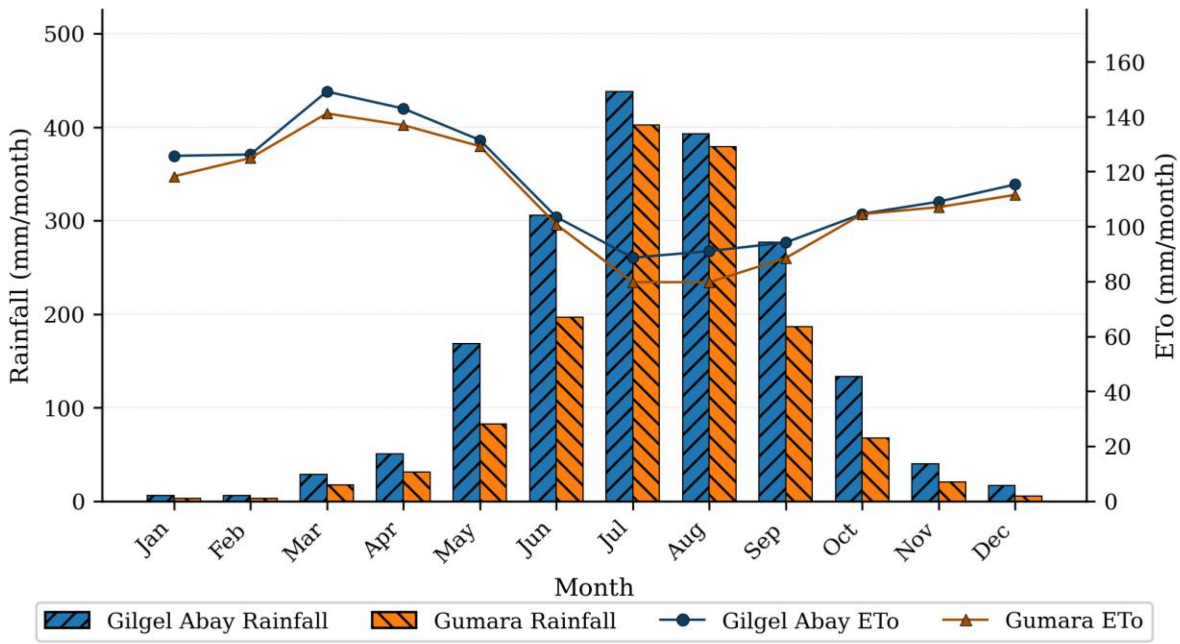

Figure 2. Average Monthly Total Precipitation (Rainfall, bar plot) and Reference Evapotranspiration (ETo, line plot) for Gilgel Abay and Gumara (1990–2020). ETo: Reference evapotranspiration estimated by Enku's simple temperature method (Enku and Melesse, 2014) (Equation 1).

The region's soils, erodible Vertisols in lower areas and Andosols in uplands, are highly susceptible to erosion, with Vertisols cracking and swelling under moisture shifts and Andosols mobilizing during intense runoff, exacerbating sediment yields (Fenta *et al.*, 2017). These processes, intensified by steep slopes, threaten the efficiency of Lake Tana's storage and the GERD (Abtew and Dessu, 2019).

To assess land use and land cover changes between 2000 and 2020 in the Gilgel Abay and Gumara watersheds, the study utilized the Global Land Analysis and Discovery (GLAD) dataset developed by the University of Maryland (Potapov *et al.*, 2022) (Figure 3). The dataset is derived from Landsat satellite imagery (Hansen *et al.*, 2013) and processed using RF classification at 30-meter spatial resolution. The annual land cover maps were made available through the GLAD Google Earth Engine (GEE) portal: (https://glad.earthengine.app/view/glcluc-2000 2020).

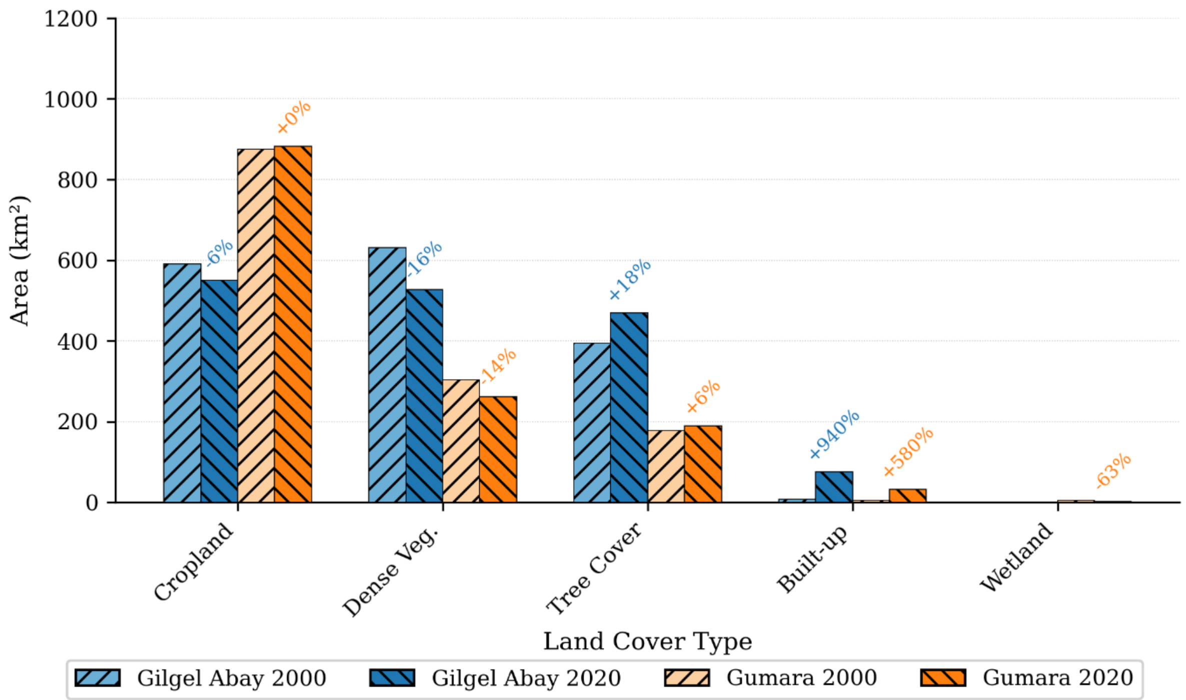

Figure 3. Land-Use and Land-Cover change Areas (km²) for Gilgel Abay and Gumara in 2000 and 2020, derived from the Global Land Analysis and Discovery (GLAD) dataset. Percentage changes are annotated above the 2020 bars.

2.2 Data collection

Hydrological, meteorological, and sediment data were collected from 1990 to 2020 for the Gilgel Abay and Gumara watersheds, at the gauging and monitoring stations listed in Table 1, to facilitate sedigraph reconstruction and sediment load analysis (Table 2). Daily discharge records, obtained from the Ethiopian Ministry of Water and Energy (MoWE) and Abay Basin Authority (ABAO) at gauging stations in Bicolo Abay (11.3500°N, 37.0167°E) for Gilgel Abay and near Woreta (11.9722°N, 37.4753°E) for Gumara, were derived from stage-discharge rating curves, calibrated biannually with field measurements during wet and dry seasons to capture seasonal variability, with gaps of 1.22% for Gilgel Abay and 2.35% for Gumara watersheds (Negatu *et al.*, 2022; Kumlachew *et al.*, 2023). Rainfall and temperature data were obtained from the Ethiopian Meteorological Institute (EMI) at ten monitoring stations (five per watershed). These stations were distributed across elevation ranges from 1,900–2,600 m a.s.l. to ensure representative spatial coverage. The rainfall records showed minor data gaps ranging from 1.5% to 3.0% during the 1990–2020 study period (Table 1). The missing rainfall percentage was quantified as the ratio of days without recorded precipitation relative to the total 10,957 days, with gaps primarily attributable to equipment malfunctions and operational challenges during data collection.

Table 1. Geographic coordinates, elevation, and missing rainfall data percentage for meteorological stations in the Gilgel Abay and Gumara watersheds (1990–2020).

Watershed	Station Name	Latitude (°N)	Longitude (°E)	Elevation (m)	Rainfall_gap (%)
Gilgel Abay	Adet	11.27	37.47	2,200	1.8
	Dangla	11.25	36.83	2,130	3
	Merawi	11.42	37.15	1,900	2.2
	Gundil	10.86	37.1	2,450	1.5
	Wetet Abay	11.37	37.03	2,300	2
Gumara	Amedber	11.91	37.89	2,350	1.9
	Wanzaye	11.76	37.63	2,100	2.7
	Mekaneyesus	11.61	38.05	2,500	2.1
	Debratabor	11.87	38.03	2,600	1.6
	Wereta	11.92	37.69	1,950	2.3

†Missing data percentage is the ratio of missing daily records to total expected daily records over the observation period.

Table 2. Summary of hydrological and sediment data for the Gilgel Abay and Gumara watersheds (1990–2020), including daily temporal resolution where applicable, with key summary statistics (minimum, median, maximum, mean) and data sources.

Parameter	Temporal Resolution	Summary Stats (Min/Median/Max)	Source
Discharge (m^3/s)	Daily	Gilgel Abay: 0.51/30.92/618.91 Gumara: 0.2/9.30/374.04	MoWE, ABAO
Rainfall (mm)	Daily	Gilgel Abay: 0.0/1.9/48.5 Gumara: 0.0/0.46/55.02	EMI
Temperature (°C)	Daily	Gilgel Abay: 10.2/18.5/26.3 Gumara: 9.8/19.1/27.0	EMI
SSC (g/L)	Intermittent	Gilgel Abay: 0.1/3.4/5.0 Gumara: 0.14/3.35/10.07	MoWE, ABAO
ETo (mm/day)	Daily	Gilgel Abay: 2.0/4.5/7.1 Gumara: 1.8/4.3/6.8	calculated

†SSC =Suspended Sediment Concentration; ETo = Reference Evapotranspiration; calculated using Enku's simple temperature method (Enku and Melesse, 2014). Statistical ranges are min: minimum, median, max: maximum; sources: Ministry of Water and Energy (MoWE), Abay Basin Authority Office (ABAO), Ethiopian Meteorological Institute (EMI).

Reference evapotranspiration (ETo) was estimated using Enku's temperature method (Enku and Melesse, 2014), based on daily maximum temperature averaged across the stations:

$$\mathrm{ET}_o = \frac{(T_{\max})^{2.5}}{48 \cdot T_{\mathrm{mm}} - 330} \qquad (1)$$

where ETo is in mm/day, T_{max} is the daily maximum temperature (°C) aggregated from five meteorological stations for each of the Gilgel Abay and Gumara watersheds, and T_{mm} (°C) is the long-term (1990–2020) daily mean maximum temperature derived from the same stations.

SSC data, provided by the MoWE and ABAO, consisted of 251 measurements for the Gilgel Abay and 245 measurements for the Gumara River, collected intermittently at the gauging stations. Sampling was strongly biased toward the wet season (June–October), reflecting monsoon-driven sediment transport peaks (Dessie *et al.*, 2015). The temporal distribution of these measurements across the 1990–2020 period was highly uneven. SSC samples were available for only 12 years for Gilgel Abay and 19 years for Gumara. Samples were heavily concentrated on a few major field campaigns, most notably 198 samples in 2012 for Gilgel Abay and 122 samples in 2016 for Gumara, with smaller numbers scattered across the early 1990s, mid-2000s, and late 2010s (Figure 4). Within the sampled years, 97.2% of Gilgel Abay and 94.3% of Gumara measurements were collected during the wet season (June–October). This patchy temporal coverage, typical of data-scarce monsoon basins where sampling is often limited to short intensive field campaigns (e.g., (Tebebu *et al.*, 2010)), implies that model generalization should be interpreted with caution for years and seasons distant from the main sampled periods. We return to this limitation in Section 4.5.

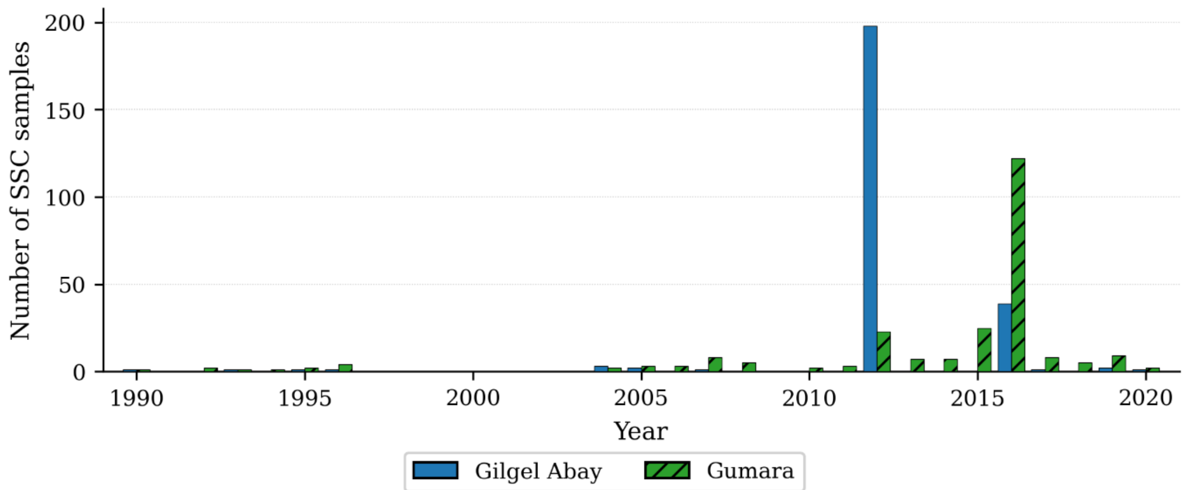

Figure 4. Temporal distribution of suspended sediment concentration (SSC) samples for the Gilgel Abay and Gumara watersheds from 1990 to 2020.

2.3 Data Pre-processing and Model Development

2.3.1 pre-processing

Pre-processing and development of the ML models were conducted for the two watersheds to reconstruct 1990–2020 sedigraphs and estimate sediment yields. Pre-processing included gap-filling, where missing discharge data were filled using an RF model trained on available discharge data, incorporating predictors such as Julian day to capture seasonal patterns, rainfall as a key driver, and lagged discharge values (1–3 days) to account for short-term runoff dynamics, which is sufficient to capture the strong day-to-day autocorrelation typical of discharge time series at this stage (Deng *et al.*, 2019). This is a shorter lag window than the 1–21-day range used in the SSC prediction models (Section 2.3.2), reflecting the different physical processes involved: discharge gap-filling primarily requires capturing short-term flow dynamics, whereas SSC prediction must additionally account for longer-memory sediment availability and supply-limited effects that can extend well beyond the discharge response itself (Guzman *et al.*, 2013). This approach, implemented in Python 3.9 with Scikit-learn 1.2, aims to improve accuracy by leveraging non-linear relationships and reducing bias from sparse temporal gaps (Jarri, 2024). Rainfall gaps were filled using the Inverse Distance Weighting (IDW) method via SciPy.stats (version 1.17.1), weighting data from ten meteorological stations (Table 1) by inverse squared distances (Virtanen *et al.*, 2020; Panigrahi, 2021).

2.3.2 Predictor Variables, Lag Selection, and Multicollinearity Control

Predictor variables for the SSC models were selected based on their physical relevance to sediment transport and the availability of continuous data. The candidate predictor set comprised: discharge-derived predictors (instantaneous discharge Q, its first difference dQ as a proxy for the rising/falling limb of the hydrograph, and a discharge hysteresis index), rainfall (P), temperature (T), reference evapotranspiration (ETo) as a soil-moisture proxy, and sine/cosine transforms of Julian day (Sin_J, Cos_J) to capture seasonal cyclicity associated with monsoon-driven sediment transport (Lund *et al.*, 2022; Almubaidin *et al.*, 2023).

Lag length selection. Catchment sediment response to a rainfall or discharge event is not instantaneous: runoff generation, hillslope-to- channel sediment delivery, and channel routing introduce delays. To characterize this delay empirically, lagged discharge and rainfall terms (Q_lag and P_lag at 1, 3, 7, 14, and 21 days) were evaluated as candidate predictors, spanning roughly three weeks of antecedent conditions. The 21-day upper bound was chosen to span the catchments' likely hydrological memory under monsoon-driven flow recession in both watersheds, while keeping the predictor set computationally manageable. Both discharge and rainfall lags were taken as candidate predictors, since antecedent rainfall, not only antecedent discharge, directly influences sediment supply through soil-moisture state and surface erodibility, and so may carry independent explanatory power for SSC beyond what discharge alone captures.

Multicollinearity control. Because discharge, its lags, and rainfall are physically coupled (rainfall generates the discharge response, and successive discharge lags are autocorrelated), the full candidate predictor set was screened for multicollinearity using the Variance Inflation Factor (VIF) before model fitting, to ensure that the overlapping information shared between discharge, rainfall, and the other hydro-meteorological inputs did not distort coefficient stability or downstream variable-importance estimates. Predictors were added iteratively, and any predictor with VIF > 10, the conventional threshold for problematic collinearity (e.g., raw instantaneous discharge Q, which was near-collinear with its own 1-day lag, VIF > 40), was excluded from the candidate pool before the iterative reduction step. Raw discharge Q was therefore represented only through its lagged values and first difference (dQ), not as a standalone predictor, eliminating the dominant source of collinearity. After this initial exclusion, the remaining 17 candidate predictors (P, T, ETo, Cos_J, Sin_J, dQ, Hysteresis, Q_lag at 1/3/7/14/21 days, P_lag at 1/3/7/14/21 days) were passed through iterative VIF reduction (threshold = 10): no further predictors exceeded the threshold in either watershed (maximum VIF = 7.61 for Gilgel Abay, 4.67 for Gumara; full VIF tables are provided in Table 3), so all 17 were retained for model training. This confirms that the retained lag structure does not introduce material redundancy between discharge- and rainfall-derived predictors.

Table 3. Variance inflation factors (VIFs) of predictor variables used in the machine-learning models for the Gilgel Abay and Gumara watersheds.

No.	Predictor	Gilgel Abay	Gumara
1	Q_lag_1	5.97	4.67
2	Q_lag_3	7.61	3.49
3	Q_lag_7	5.2	2.66
4	Q_lag_14	5.49	2.61
5	Q_lag_21	5.78	2.7
6	P	1.53	1.84
7	P_lag_1	1.54	1.86
8	P_lag_3	1.51	1.59
9	P_lag_7	1.43	1.57
10	P_lag_14	1.32	1.38
11	P_lag_21	1.35	1.5
12	T	1.55	1.3
13	ETo	1.71	2.81
14	dQ	1.71	1.93
15	Hysteresis	1.73	1.69
16	Sin_J	6.95	2.25
17	Cos_J	2.74	4.32

Target variable bounding. Predicted SSC was constrained to the range of the observed SSC record for each watershed: 0.01–5.0 g/L for Gilgel Abay and 0.01–10.07 g/L for Gumara, corresponding to the minimum and maximum SSC values measured during the 1990–2020 sampling period (Table 2). Because these bounds equal the true observed extremes, this step does not alter any observed SSC value used in model fitting; by definition, no measurement exceeds its own dataset's maximum, and instead only constrains the model's out-of-sample predictions, preventing extrapolation beyond the physically observed sediment concentration range for unmeasured days. The lower bound (0.01 g/L) additionally avoids non-physical zero or negative values during the log-based transformation used by the SRC baseline (Equation 2).

Variable importance and ablation. To assess the influence of each retained predictor independent of the collinearity already controlled for above, permutation-free feature importance (mean decrease in impurity, MDI) was computed from the trained QRF, the best-performing model (Section 3.1), for each watershed. Because the predictor set entering this step was already VIF-filtered, the resulting importance ranking reflects each variable's contribution net of the strongest correlated alternatives, rather than importance that is partly attributable to a collinear proxy, an ablation-style assessment of input variable importance that is not confounded by inter-predictor correlation. Across both watersheds, this VIF-independent ranking confirms that discharge, rainfall, and their multi-day lags each retain distinct explanatory power once collinearity is controlled for, but with different leading terms per watershed: short-lag rainfall and the seasonal cosine term dominate in Gilgel Abay, while ETo, temperature, and the 1-day discharge lag dominate in Gumara (Section 3.2), rather than a single variable dominating universally.

Recurrent/sequence models. Recurrent sequence architectures (e.g., Long Short-Term Memory, LSTM, networks), which can learn lag structure directly from data rather than through pre-specified lag terms, were not evaluated in this study. Model comparison was restricted to the SRC, GB, RF, and QRF architectures described above, each optimized under the common hyperparameter-search protocol in Section 2.3.3. This scope decision is discussed further in Section 4.5.

2.3.3 Model Training, Hyperparameter Optimization, and Validation Strategy

The dataset (n = 251 daily samples for Gilgel Abay; n = 245 for Gumara, selected as the longest continuous run of dates with no missing values across all retained predictors and the SSC target) was split into 70% training and 30% testing subsets using a single random split (*scikit-learn train_test_split, random_state = 42*, shuffled).

All continuous predictors were standardized (zero mean, unit variance) using *scikit-learn StandardScaler*, fit on the training subset only and applied to the test subset using the training-subset statistics to prevent information from the test set leaking into the scaling transformation. Four modeling approaches were trained to predict daily SSC: a Sediment Rating Curve (SRC), Gradient Boosting (GB), Random Forest (RF), and Quantile Random Forest (QRF). The SRC was fitted via log–log least-squares regression (SciPy) on each side of a discharge threshold set at the median training-set discharge (Equation 2) and required no hyperparameter search. For GB, RF, and QRF, hyperparameters were optimized using randomized search (scikit-learn *RandomizedSearchCV*, 15–20 sampled configurations per model) combined with 10-fold cross-validation (*scikit-learn KFold*, shuffled, *random_state = 42*) on the training subset, with R^2 as the scoring metric. The final selected configuration for each model and watershed is reported in Table 4 (e.g., for QRF, the searched hyperparameter ranges are: *n_estimators* ∈ {500, 1000, 2000}, *max_depth* ∈ {10, 20, 30}, *min_samples_split* ∈ {2, 5}, *min_samples_leaf* ∈ {1, 2, 3}, *max_features* ∈ {$\sqrt{p}$, 0.5, 0.8}). Constraining tree depth, the minimum samples per split/leaf, and the fraction of features considered at each split served as the primary regularization mechanisms that controlled model complexity (see Overfitting Control, below).

Table 4. Optimized hyperparameter values for the Gradient Boosting (GB), Random Forest (RF), and Quantile Random Forest (QRF) models developed for the Gilgel Abay (GA) and Gumara (GU) watersheds.

Hyperparameter	GB (GA)	GB (GU)	RF (GA)	RF (GU)	QRF (GA)	QRF (GU)
n_estimators	500	500	500	500	1000	2000
max_depth	3	5	10	10	10	30
min_samples_split	5	5	2	2	5	5
min_samples_leaf	5	2	2	1	3	1
max_features	–	–	sqrt	sqrt	sqrt	0.5
learning_rate	0.05	0.05	–	–	–	–
subsample	0.7	0.7	–	–	–	–

† (GA = Gilgel Abay; GU = Gumara)

Cross-validation and temporal dependence. The standard K-fold cross-validation with shuffling does not preserve temporal ordering, and hydrological time series can exhibit autocorrelation that shuffled K-fold does not explicitly account for. We retained a shuffled K-fold rather than a blocked/forward-chaining temporal split for two reasons specific to this dataset. First, the 251/245-sample training data, after restricting to the longest contiguous run of complete records across all 17 VIF-filtered predictors, already represents a much-reduced, gap-constrained subset of the full 1990–2020 record rather than a long, densely sampled continuous sequence; a contiguous-block temporal split on a series this short would leave individual folds too small to reliably estimate held-out R^2 (commensurate with the use of cross-validation for hyperparameter selection rather than for the final reported test-set performance, which used a single, fixed split). Second, the predictor set used for training already encodes temporal structure explicitly through the multi-scale lag features (1–21 days), discharge hysteresis, and seasonal Julian-day terms, so each training row carries information about its recent antecedent conditions independent of fold assignment, which reduces (though does not eliminate) the risk that shuffled folds simply memorize seasonal position. We nonetheless flag shuffled K-fold as a methodological simplification: a blocked or *TimeSeriesSplit*-style cross-validation scheme remains preferable in principle for hydrological series and is noted as a direction for future refinement of this pipeline in Section 4.5.

Leakage prevention. Two additional steps were taken to limit train/test leakage beyond the train-only *StandardScaler* fit described above: (i) all lagged predictor columns were constructed on the full, date-sorted series before the train/test split, so that lag values for a given date are always computed from genuinely antecedent observations rather than from values that could include post-split information; and (ii) the single train/test split used for final reported performance (Section 3.1) is distinct from, and was not reused as, any of the 10 cross-validation folds used during hyperparameter selection, the test subset was held out before and independent of the *RandomizedSearchCV* procedure.

2.3.4 Overfitting Control

A gap was observed between training and validation performance (training R^2 up to 0.89, while validation R^2 for the ensemble models ranged from 0.66–0.75 range for some model/watershed combinations), indicating that model complexity was not fully constrained by regularization alone. The following measures were applied to mitigate this:

- Explicit complexity constraints on all tree-based models via the hyperparameter search space described above, bounding *max_depth*, enforcing minimum samples per split (*min_samples_split*) and per leaf (*min_samples_leaf*), and restricting the feature subset considered at each split (*max_features*), each of which directly limits the capacity of individual trees to fit training-set noise.
- Subsampling for Gradient Boosting (*subsample* $\in \{0.7, 0.9\}$), which fits each boosting stage on a random subset of the training data, is a standard stochastic-regularization technique for boosted trees.
- Early stopping for Gradient Boosting via *n_iter_no_change* = 10 with a held-out *validation_fraction* = 0.1 carved from the training subset, halting boosting once

validation loss stopped improving for 10 consecutive iterations, rather than fitting a fixed, potentially excessive number of stages.

- Cross-validated hyperparameter selection (Section 2.3.3) ensured that the reported configuration was the one generalizing best across 10 held-out folds during search, rather than the configuration minimizing training error.

Model development was implemented in Python 3.9 using Scikit-learn 1.2, QuantileForest 1.3, SciPy 1.8, and Matplotlib 3.5 (Meinshausen, 2006; Hunter, 2007; Pedregosa *et al.*, 2011; Virtanen *et al.*, 2020). Four modeling approaches were employed to predict daily SSC, each selected for its distinct capabilities in addressing varied challenges of sedigraph reconstruction. The SRC served as a baseline due to its simplicity in representing SSC–discharge relationships based on a power law relationship (Equation 2), despite well-known limitations under non-linear conditions (Asselman, 2000).

$$\mathrm{SSC} = a \cdot Q^b \tag{2}$$

Where Q is discharge (m^3/s) and a and b are coefficients, fitted via least-squares regression in SciPy. SRCs used log-transformed discharge to stabilize variance or capture hydrological variability (Asselman, 2000; Horowitz, 2003).

RF and GB, each with 1,000–5,000 trees and tuned hyperparameters (e.g., max_depth, min_samples_split, max_features), were selected for their ability to capture complex, multivariate SSC responses under data scarcity (Nourani *et al.*, 2019; AlDahoul *et al.*, 2022). QRF, with similar hyperparameter tuning, was employed to model conditional quantiles (0.05, 0.25, 0.5, 0.75, 0.95), enabling uncertainty quantification for risk-informed sediment management (Meinshausen, 2006).

The land cover data processing and analysis were carried out within the GEE cloud computing platform. The land cover maps were clipped to the boundaries of the Gilgel Abay and Gumara watersheds using uploaded Feature Collection shapefiles. Frequency histograms were generated to quantify the number of pixels per land cover class, which were then converted into area measurements (km^2) based on the 30 m spatial resolution. The classification scheme used by GLAD is consistent across years and supported by a comprehensive legend, ensuring cross-year comparability. The extracted results were exported to Google Drive in CSV format for post-processing and visualization.

2.4 Sedigraph Reconstruction and Sediment Yield Estimation

Sedigraph reconstruction and sediment yield estimation for both watersheds were performed using the optimized QRF model from Section 2.3 to generate continuous 1990–2020 sedigraphs and quantify sediment dynamics. The QRF was selected for final sedigraph reconstruction based on its validation performance relative to the other three models (Section 3.1), and for its ability to provide uncertainty quantification, predicting daily SSC from the median (0.5 quantiles) of trained conditional quantiles (0.05, 0.25, 0.5 0.75, 0.95), using the VIF filtered predictor set described in Section 2.3.2 to capture monsoon-driven variability and seasonal cyclicity (Meinshausen and Ridgeway, 2006).

Daily sediment loads were estimated by multiplying predicted SSC (g/L) by daily discharge (m^3/s) and converting to tonnes/day using the factor 86.4:

$$\text{Load} = \text{SSC} \cdot Q \cdot 86.4 \qquad (3)$$

Where Load is in tonnes/day, SSC is in g/L, Q is discharged in m^3/s, and 86.4 converts g/s to tonnes/day (seconds/day ÷ 10^6 g/ton).

Annual and seasonal (wet and dry) sediment yields were computed by aggregating daily loads and normalizing by watershed areas (166,400 ha for Gilgel Abay, 139,400 ha for Gumara), expressed as tonnes per hectare per year (t/ha/yr) (Worku *et al.*, 2025). This approach enabled the identification of peak sediment events and supported the assessment of land-use impacts on erosion, providing critical data for managing Lake Tana’s storage and the GERD's operational resilience (Abtew and Dessu, 2019).

3. RESULTS

This section presents the performance of four models, SRC, GB, RF, and QRF, in predicting daily SSC and reconstructing sedigraphs for the Gilgel Abay and Gumara watersheds in the UBNB (1990–2020). Using 251 (Gilgel Abay) and 245 (Gumara) SSC measurements with continuous predictors (Section 2.3), we report model performance, feature importance, sediment yields (annual, monthly, seasonal scales), and correlations with land-use and land-cover (LULC) changes from GLAD data (Sections 3.1–3.5).

3.1 Model Performance and Selection

QRF outperformed SRC, GB, and RF in predicting SSC, achieving high accuracy with training R^2 values of 0.85 for Gilgel Abay and 0.89 for Gumara and validation R^2 values of 0.73 and 0.75, mean absolute errors (MAE) of 0.44 and 0.45 g/L, root mean squared error (RMSE) of 0.59 and 0.62 g/L, mean absolute percentage error (MAPE) of 25.0% and 20.8%, respectively

(Table 5). In contrast, SRC showed the lowest performance (validation R² = 0.20/0.19, MAE = 0.87/0.48 g/L), while GB and RF showed intermediate results (validation R² = 0.67–0.71, Table 5). QRF's superior performance resulted from its ability to model non-linear SSC dynamics and seasonal cyclicity for monsoon-driven variability. Model selection was based jointly on training-set fit, held-out validation R², and the error metrics (MAE, RMSE, MAPE) summarized in Table 5; Figure 5 shows the training-set observed-versus-predicted scatter for all four models, illustrating each model's ability to capture the observed non-linear SSC-discharge relationship, while Figure 6 presents the corresponding validation R² comparison that guided final model selection. Using conditional quantiles, QRF generated daily SSC predictions from 1990–2020 for the two watersheds, validated against the held-out 30% test subset with uncertainty bounds from the 0.05 and 0.95 conditional quantiles.

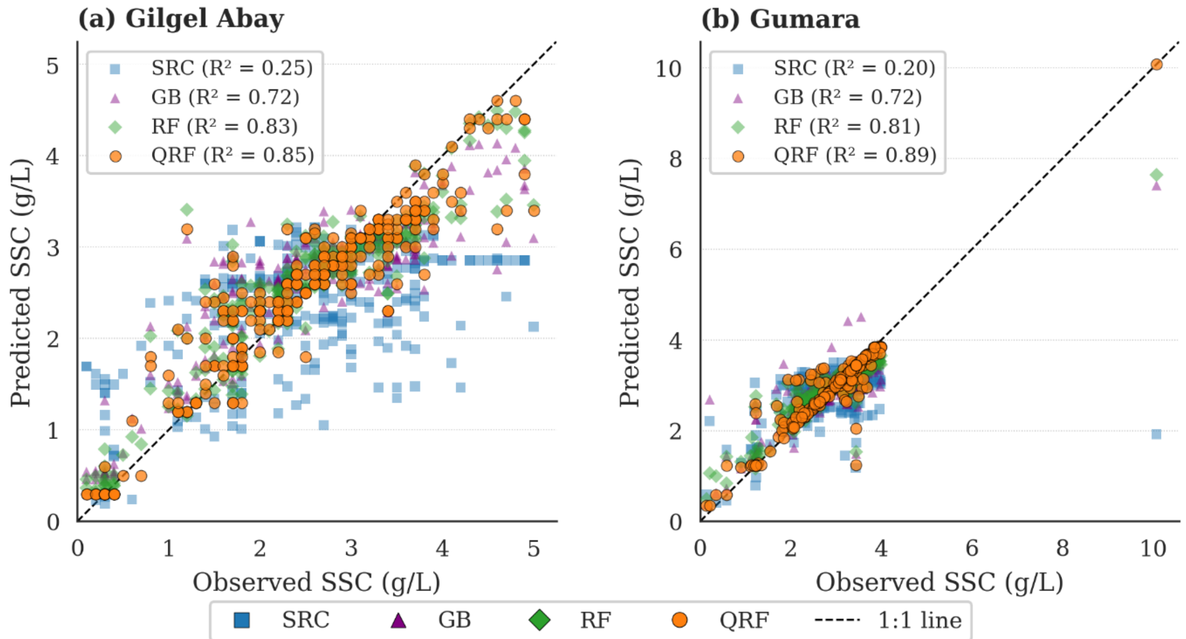

Figure 5. Observed vs. Predicted Suspended Sediment Concentration (SSC, g/L) on the training subset for (a) Gilgel Abay and (b) Gumara (1990–2020); R² values shown are training-set fit. Held-out validation R² and error metrics for the same models are reported in Table 5 and Figure 6. SRC: Sediment Rating Curve; GB: Gradient Boosting; RF: Random Forest; QRF: Quantile Random Forest.

Table 5. Model performance in predicting suspended sediment concentration in the Gilgel Abay and Gumara watersheds (1990–2020) using Sediment Rating Curve (SRC), Gradient Boosting (GB), Random Forest (RF), and Quantile Random Forest (QRF). Metrics include training and validation coefficient of determination (R^2), mean absolute error (MAE), root mean squared error (RMSE), and mean absolute percentage error (MAPE). The QRF model achieved the highest accuracy across both watersheds. Bold values indicate the best performed value and model.

Watershed	Model	Training R²	Validation R²	RMSE (g/L)	MAE (g/L)	MAPE (%)
	SRC	0.25	0.2	0.96	0.87	58.48
Gilgel Abay	GB	0.72	0.67	0.65	0.50	32.16
	RF	0.83	0.71	0.61	0.44	28.41
	QRF	**0.85**	**0.73**	**0.59**	**0.44**	**25.03**
	SRC	0.20	0.19	0.63	0.48	22.73

Gumara	GB	0.72	0.66	0.61	0.48	22.1
	RF	0.81	0.70	0.60	0.44	21.13
	QRF	**0.89**	**0.75**	**0.62**	**0.45**	**20.8**

Figure 6 presents a bar chart comparing validation R^2 values for SRC, GB, RF, and QRF across Gilgel Abay and Gumara, highlighting QRF's superior performance (R^2 = 0.73/0.75). This complements Figure 5, which shows scatter plots of observed versus predicted SSC, illustrating QRF's tighter clustering around observed values.

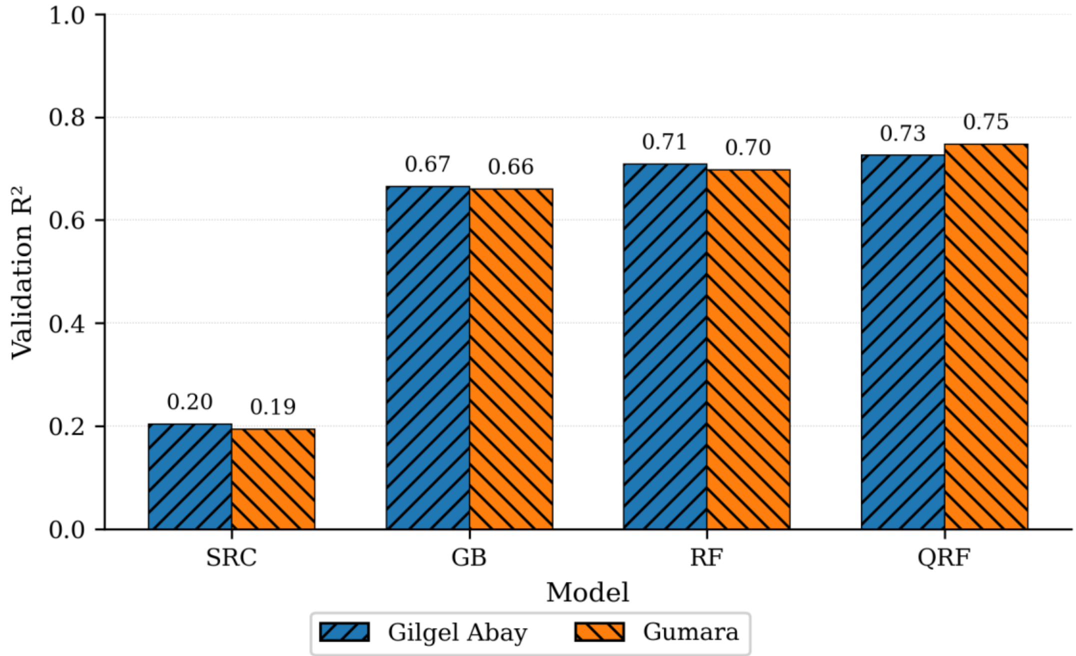

Figure 6. Comparison of model performance based on validation R^2 for SSC Prediction Models (SRC, GB, RF, QRF) in Gilgel Abay and Gumara (1990–2020). SRC: Sediment Rating Curve; GB: Gradient Boosting; RF: Random Forest; QRF: Quantile Random Forest; SSC: Suspended Sediment Concentration.

3.2 Feature Importance

Feature importance from the QRF model, computed as mean decrease in impurity (MDI) on the VIF-filtered, 17-predictor set described in Section 2.3.2, differed markedly between the two watersheds (Figure 7; Table 6). For Gilgel Abay, the leading predictors were rainfall-lag terms: a 1-day rainfall lag (P_lag_1, MDI = 0.15) ranked highest, followed by the seasonal cosine term (Cos_J, 0.13), a 3-day rainfall lag (P_lag_3, 0.12), and the 1-day discharge lag (Q_lag_1, 0.09). This rainfall-forward ranking is consistent with Gilgel Abay's stronger Pearson correlations between SSC and short-lag rainfall (P_lag_1: r = 0.54; P_lag_3: r = 0.49; Table 7) relative to discharge lags (Q_lag_1: r = 0.38; Table 7). For Gumara, by contrast, reference evapotranspiration (ETo, MDI = 0.15), temperature (T, 0.13), a 7-day rainfall lag (P_lag_7, 0.12), and the 1-day discharge lag (Q_lag_1, 0.12) carried the greatest weight, pointing to a sediment response shaped more strongly by discharge and atmospheric-demand variables, consistent with Gumara's comparatively stronger SSC-discharge correlation (Q_lag_1: r = 0.41; Table 7). Across both watersheds, the discharge first difference (dQ) and the hysteresis index contributed the least (MDI < 0.03 in both watersheds; Table 6), indicating that instantaneous rate-of-change and loop-rating effects add comparatively little explanatory power once the multi-scale lag structure is already represented among the retained predictors. Because the predictor set entering this analysis was already VIF-filtered (Section 2.3.2), these importance rankings reflect each variable's contribution net of the strongest collinear alternatives rather than importance partly attributable to a correlated proxy. These watershed-specific rankings, interpreted further in Section 4.2, indicate that Gilgel Abay's sediment response is more strongly paced by rainfall, whereas Gumara's is more strongly shaped by antecedent discharge and evaporative demand.

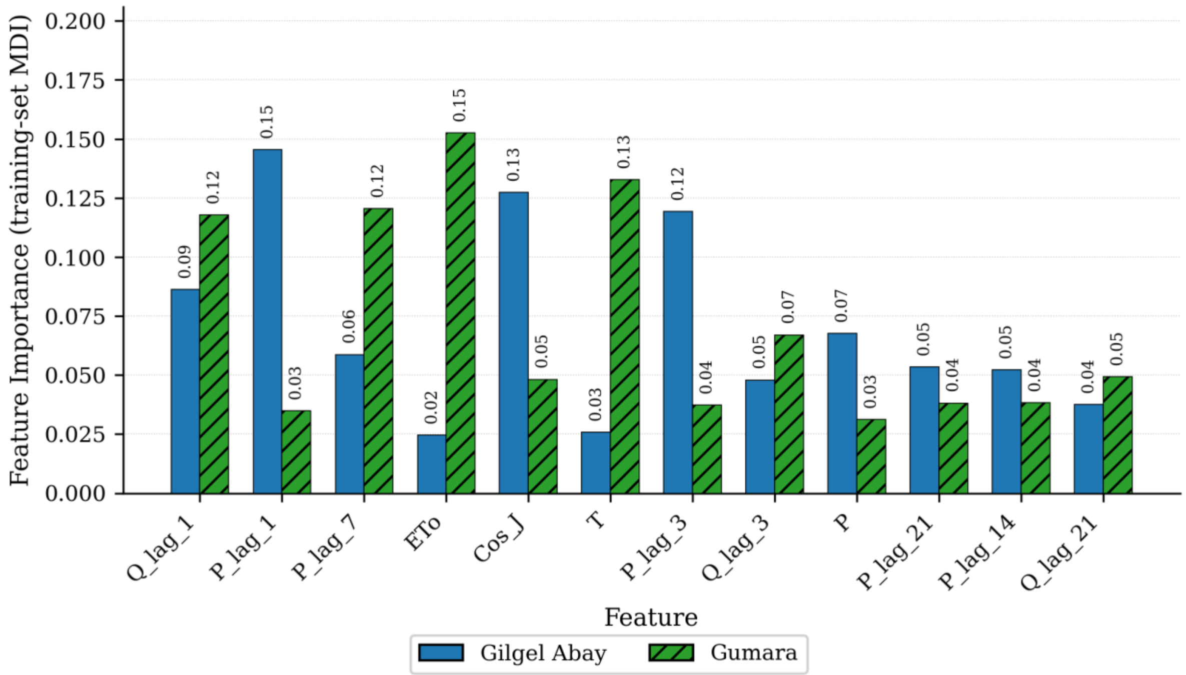

Figure 7. Feature importance (Mean Decrease in Impurity, MDI) of the top 12 predictors for suspended sediment concentration (SSC) prediction in the Gilgel Abay and Gumara watersheds using the Quantile Random Forest model. The five least important features (all with MDI ≈ 0.04–0.05) are not shown for clarity. The full ranking for all 17 predictors is available in Table 6.

Table 6. The full ranking of all 17 VIF-filtered predictors for feature importance (Mean Decrease in Impurity, MDI) of predictor variables for suspended sediment concentration (SSC) prediction in the Gilgel Abay and Gumara watersheds from the Quantile Random Forest (QRF) model.

No.	Feature	Gilgel Abay	Gumara
1	Q_lag_1	0.086	0.118
2	P_lag_1	0.145	0.035
3	P_lag_7	0.059	0.120
4	ETo	0.025	0.153

5	Cos_J	0.127	0.048
6	T	0.026	0.133
7	P_lag_3	0.119	0.037
8	Q_lag_3	0.048	0.067
9	P	0.068	0.031
10	P_lag_21	0.053	0.038
11	P_lag_14	0.052	0.038
12	Q_lag_21	0.038	0.049
13	Q_lag_7	0.045	0.040
14	Sin_J	0.059	0.023
15	Q_lag_14	0.033	0.041
16	dQ	0.015	0.028
17	Hysteresis	0.002	0.001

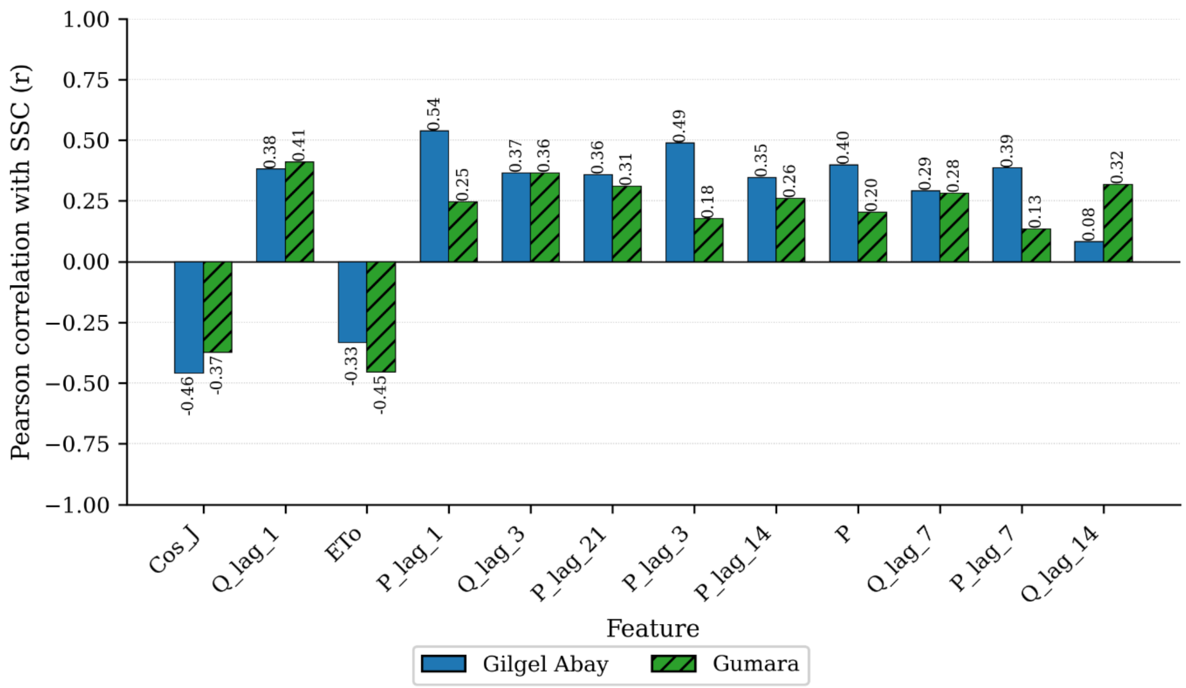

Figure 8. Pearson correlation coefficients between predictors and observed suspended sediment concentration (SSC) for the Gilgel Abay and Gumara watersheds. The top 12 predictors ranked by mean absolute correlation are shown. The five weakest predictors are omitted for clarity.
† Positive values indicate direct relationships, while negative values indicate inverse relationships.
‡ Abbreviations: QRF, Quantile Random Forest; SSC, Suspended Sediment Concentration; Q_lag_1/3/7/14/21, discharge lagged by 1/3/7/14/21 days; P_lag_1/3/7/14/21, rainfall lagged by 1/3/7/14/21 days; dQ, first difference of discharge; ETo, reference evapotranspiration; T, temperature; Sin_J/Cos_J, sine/cosine transform of Julian day; VIF, variance inflation factor. Full VIF and correlation results for all 17 retained predictors are provided in Table 3.

Table 7. Pearson correlation coefficient between key predictors and Suspended Sediment Concentration (SSC) for the Gilgel Abay and Gumara watersheds (1990–2020).

No.	Predictor	Gilgel Abay (r)	Gumara (r)
1	P_lag_1	0.538	0.246
2	P_lag_3	0.488	0.176

3	P	0.399	0.203
4	P_lag_7	0.386	0.134
5	Q_lag_1	0.381	0.41
6	Q_lag_3	0.365	0.365
7	P_lag_21	0.358	0.31
8	P_lag_14	0.346	0.261
9	Q_lag_7	0.292	0.283
10	dQ	0.104	0.064
11	Q_lag_14	0.082	0.317
12	Hysteresis	0.051	0.089
13	Q_lag_21	0	0.279
14	Sin_J	-0.16	-0.15
15	T	-0.257	-0.135
16	ETo	-0.334	-0.454
17	Cos_J	-0.46	-0.374

3.3 Annual and Monthly Sediment Yields

The reconstructed sedigraphs for both watersheds are shown in Figure 9. The QRF model reproduces the characteristic monsoon-driven seasonal cycle throughout the 1990–2020 record for both watersheds, with sharp annual SSC rises during the wet season (June–October) followed by recession toward low dry-season baseflow concentrations. Within the densely sampled periods, most notably 2012–2013 and 2016 for Gilgel Abay, and the more distributed sampling across 1990–2020 for Gumara (Section 2.2; Figure 4), reconstructed SSC tracks observed values closely, including during the largest observed peaks (e.g., the 2012–2013 Gilgel Abay event and the 1993 Gumara peak exceeding 10 g/L). For years and periods without observed measurements, the reconstructed series reflects the model's learned relationship between SSC and the hydro-meteorological predictors (Section 2.3) rather than direct validation against measured sediment concentration; given the uneven temporal distribution of SSC sampling documented in Section 2.2 and Figure 4, reconstructed values in sparsely sampled years should be interpreted as model-consistent estimates rather than independently verified observations, a limitation discussed further in Section 4.5. Reconstructed SSC for Gilgel Abay is bounded at 5.0 g/L and for Gumara at 10.07 g/L, corresponding to the maximum SSC concentrations observed in each watershed's 1990–2020 measurement record (Table 2; Section 2.3); as a result, the flat-topped peaks visible in panel (a) around 2012–2013 reflect this empirically grounded ceiling; the highest sediment concentration ever measured in that catchment; rather than an arbitrary cap or an unconstrained model prediction.

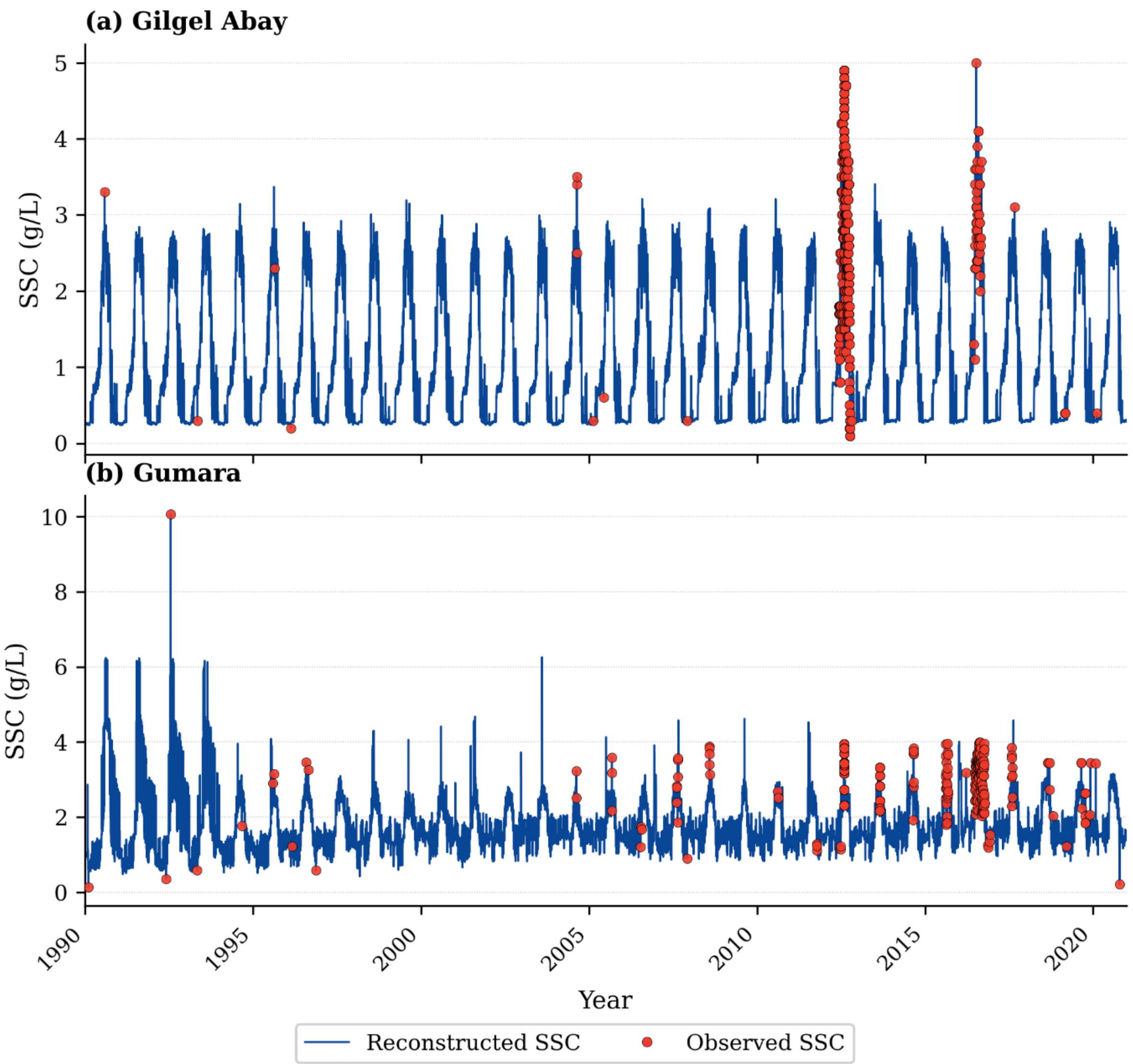

Figure 9. Reconstructed daily suspended sediment concentration (SSC) time series and observed SSC values for (a) Gilgel Abay and (b) Gumara watersheds (1990–2020).

The reconstructed QRF-predicted annual sediment yields were estimated at 30.7±7.2 t/ha/yr (Gilgel Abay) and 27.5±10.74 t/ha/yr (Gumara), with peaks at 48.5 (2018, Gilgel Abay) and 40.2 t/ha/yr (2020, Gumara) (Figure 10). Mean and standard deviation (std, mean ± std). Monthly sediment yields were 2.3±3.0 t/ha/month for Gilgel Abay and 2.1±3.3 t/ha/month for Gumara, with peaks during the core wet season months (June–September) reaching 8.7 t/ha/month (Gilgel Abay) and 10.5 t/ha/month (Gumara) (Figure 11). Gilgel Abay's yields were driven by high peak discharge (618.9 m^3/s, specific discharge 0.0037 $m^3/s/ha$) and rapid urbanization (940% built-up area increase, 2000–2020). Gumara's yields, with greater variability (std = 3.3 t/ha/month), were influenced by intense rainfall (max 531.8 mm/month), urbanization (580% built-up area increase), and 63% wetland loss (2000–2020) (Table 8).

These patterns, supported by 372 monthly measurements per watershed, confirm QRF's sensitivity to monsoon-driven dynamics within the wet season (June–October; Figure 11).

Figure 10. Annual Rainfall (mm), Discharge (m³/s), and Sediment Yield (t/ha/yr) with IQR for (a) Gilgel Abay, (b) Gumara (1990–2020). SSC: Suspended Sediment Concentration; QRF: Quantile Random Forest; IQR: Interquartile Range.

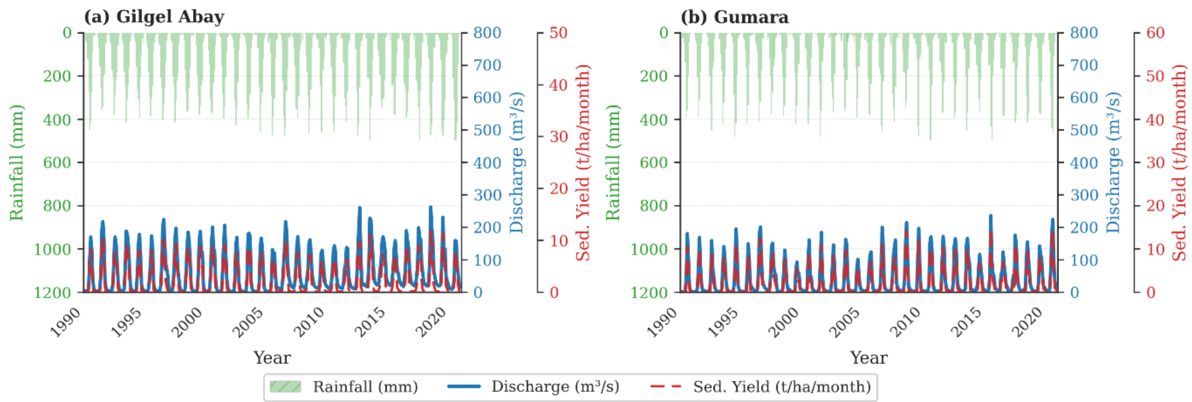

Figure 11. Monthly Rainfall, Discharge, and Sediment Yield for (a) Gilgel Abay and (b) Gumara (1990–2020).

3.4 Seasonal Sediment Yields

Seasonal sediment yields, estimated for an extended wet season (June–October, 153 days/season) and dry season (November–May, 212 days/season) using the optimized QRF configuration for each watershed (Table 4: n_estimators = 1000, max_depth = 10, max_features = sqrt for Gilgel Abay; n_estimators = 2000, max_depth = 30, max_features = 0.5 for Gumara). For Gilgel Abay, wet season sediment yields were estimated at 24.8 t/ha/yr (Q25: 19.6, Q75:31.7), contributing 95% of annual yields, while dry season yields averaged 1.0 t/ha/yr (Q25: 0.7, Q75: 1.6). For Gumara, wet season yields averaged 22.4 t/ha/yr (Q25:18.3, Q75:25.9), contributing 96% of annual yields, with dry season yields averaging 1.1 t/ha/yr (Q25: 0.8, Q75: 1.6) (Figure 12). The wet and dry season reported here are medians of the reconstructed daily sediment yield distribution within each season, with the accompanying interquartile range reflecting inter-annual variability; because a median does not sum additively the way a mean does, these two seasonal medians are not expected to add up to the annual mean reported in Section 3.3. The wet season contribution percentages (95%, 96%) were instead calculated by partitioning the total reconstructed sediment load (Equation 3) by season and dividing by the annual total, consistent with the mean based annual yields reported above. The extended wet season includes October to capture residual monsoonal runoff, ensuring accurate classification of high-yield periods driven by intense rainfall (97.2% and 94.3% of the 251 Gilgel Abay and 245 Gumara SSC measurements, respectively, fell within wet-season sampled years; Section 2.2) and peak flows (618.9 m³/s for Gilgel Abay, 496.3 m³/s for Gumara). These patterns highlight the wet season's dominant role in erosion, validate the accuracy of QRF (validation R^2 = 0.73 for Gilgel Abay, 0.75 for Gumara; Section 3.1) in modeling sediment dynamics, and highlight the need for targeted wet-season erosion control measures to protect Lake Tana and the GERD.

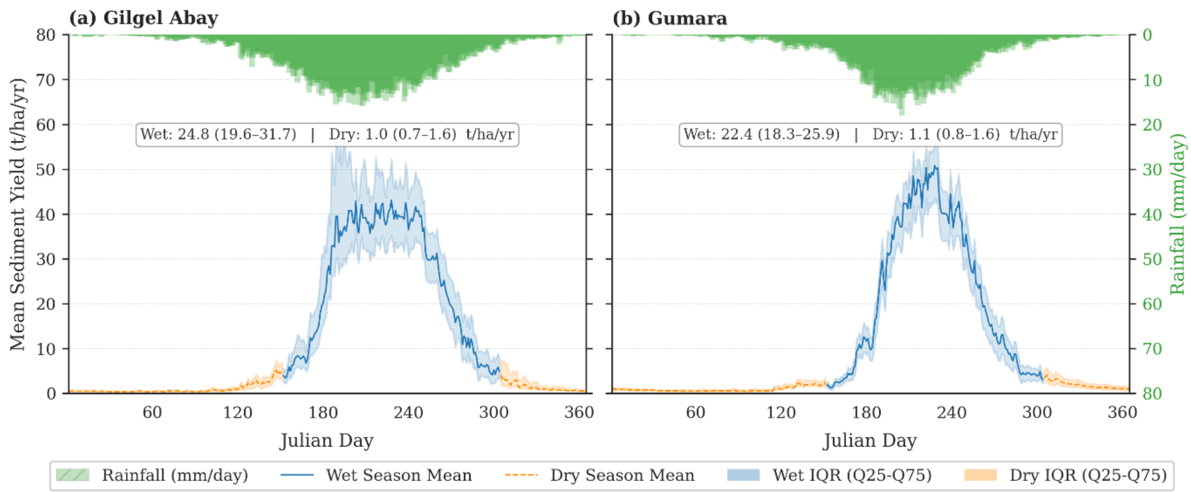

Figure 12. Seasonal Rainfall and Median Sediment Yield with Interquartile Range (IQR) for (a) Gilgel Abay and (b) Gumara (1990–2020). Rainfall (mm), Wet Season Sediment Yield (t/ha/yr), Dry Season Sediment Yield (t/ha/yr). Values shown are medians; see Section 3.4 for the relationship to the annual mean yields in Section 3.3.

3.5 Land-Use and Land-Cover Correlations

LULC changes, derived from GLAD data (2000–2020), showed significant correlations with annual sediment yields in Gilgel Abay and Gumara watersheds (Table 8). Built-up areas increased by 940% in Gilgel Abay (7.3 to 76 km^2) and 580% in Gumara (4.6 to 32 km^2), with a moderate positive correlation in Gilgel Abay ($r = 0.39$, $p = 0.08$) and a strong positive correlation in Gumara ($r = 0.84$, $p < 0.0001$). In Gumara, the wetland area decreased by 63% (4.4 to 1.6 km^2), showing a strong negative correlation with sediment yield ($r = -0.84$, $p < 0.0001$), likely due to reduced soil retention capacity. Cropland decreased slightly in Gilgel Abay (590 to 551 km^2, -6%) but remained stable in Gumara (875 to 882 km^2, 0%). Dense short vegetation declined by 16% in Gilgel Abay and 14% in Gumara, while tree cover increased by 18% and 6%, respectively. These LULC plots are visualized in Figure 3 and linked to increased runoff in Gumara with a peak discharge of 496.3 in 2020. Figure 13 illustrates the correlations between sediment yield and interpolated built-up areas (Gilgel Abay and Gumara), highlighting urbanization's role in enhancing erosion in Gumara ($r = 0.84$) and a weaker association in Gilgel Abay ($r = 0.39$).

Because the QRF model was trained exclusively on hydro-meteorological predictors (discharge- and rainfall-derived lags, temperature, ETo, and seasonal indicators; Section 2.3.2) and does not incorporate LULC variables, the sediment yields correlated with LULC change here are model-derived estimates that do not themselves encode land-use information. These correlations are therefore descriptive and hypothesis-generating rather than causal (see Section 4.4 for further discussion).

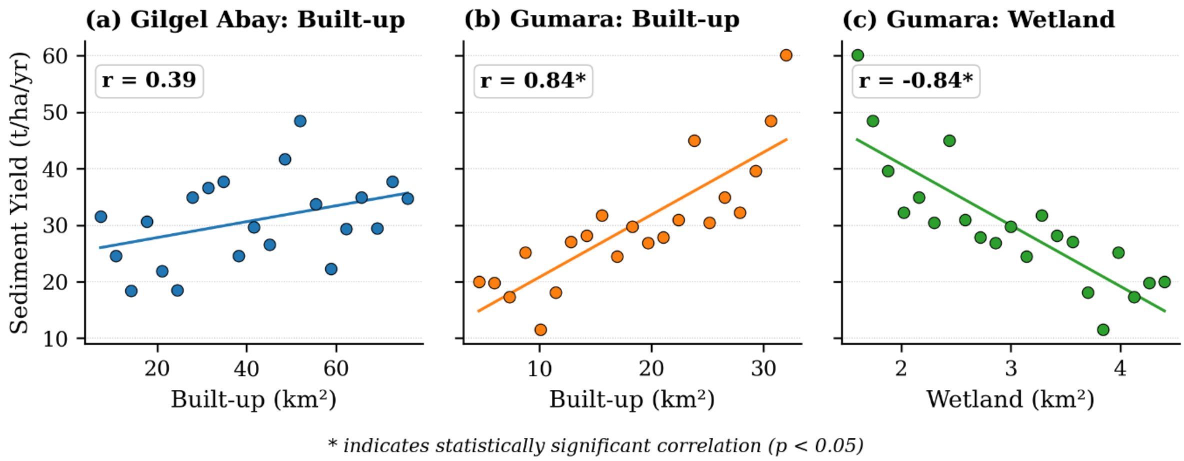

Figure 13. Relationships between Annual Sediment Yield (t/ha/yr) and Land Use Components (2000–2020). (a) Gilgel Abay Built-up Area, (b) Gumara Built-up Area, (c) Gumara Wetland Area. Pearson correlation coefficients (r) are shown in each panel.

Table 8. Land-use and Land-cover (LULC) changes in the Gilgel Abay and Gumara watersheds between 2000 and 2020 derived from the Global Land Analysis and Discovery (GLAD) datasets. Area values are in km^2, with the percentage change reflecting the relative difference over the 20 years.

Watershed	Land Cover Type	Area in 2000 (km^2)	Area in 2020 (km^2)	Change (%)
Gilgel Abay	Cropland	590	551	-6%
	Dense short vegetation	631	527	-16%
	Tree cover	394	469	18%
	Built-up	7.3	76	940%
Gumara	Cropland	875	882	0%
	Dense short vegetation	304	261	-14%
	Tree cover	178	190	6%
	Built-up	4.6	32	580%
	Wetland	4.4	1.6	-63%

4. DISCUSSION

4.1 Model Performance and Selection

The QRF model demonstrated superior performance over GB, RF, and SRC in predicting SSC for both the Gilgel Abay and Gumara watersheds. For Gilgel Abay, QRF achieved the highest validation R^2 (0.73) and the lowest mean absolute error (MAE = 0.44 g/L), outperforming GB (validation R^2 = 0.67, MAE = 0.50 g/L), RF (validation R^2 = 0.71, MAE = 0.44 g/L), and SRC (validation R^2 = 0.20, MAE = 0.87 g/L). Similarly, for Gumara, QRF attained a validation R^2 of 0.75 and MAE of 0.45 g/L, compared with GB (R^2 = 0.66, MAE = 0.48 g/L), RF (R^2 = 0.70, MAE = 0.44 g/L), and SRC (R^2 = 0.19, MAE = 0.48 g/L; Table 5; Figure 5).

This superior performance is attributed to QRF's quantile-based approach, which effectively captures non-linear sediment dynamics and heteroscedasticity (uneven error variance; (Zhang *et al.*, 2022b)), particularly during peak discharge events (618.9 m^3/s for Gilgel Abay and 496.3 m^3/s for Gumara; Section 3.4). These results align with previous studies highlighting the advantages of ensemble tree-based models in hydrological applications (Nourani *et al.*, 2019; AlDahoul *et al.*, 2022). Recent research further confirms that machine learning methods, such as XGBoost, consistently outperform traditional sediment rating curves and enable projections under climate change scenarios (Bezak *et al.*, 2025). Incorporating time-varying sediment availability into the rating-curve framework, rather than relying on discharge alone, has been shown to substantially improve rating-curve performance in non-stationary systems (Zhang *et al.*, 2021), suggesting a possible refinement of the SRC baseline for future applications in the UBNB.

In contrast, the SRC model, which relies on a simple power law relationship between discharge and SSC, exhibited the weakest performance, highlighting the limitation of empirical models in complex monsoon-dominated systems (Asselman, 2000; Francke *et al.*, 2008). Overfitting was mitigated, though not fully eliminated (Section 2.3.4), through a random 70/30 train-test split, cross-validated hyperparameter selection, and complexity constraints (min_samples_split = 2–5, min_samples_leaf = 1–3), narrowing the training–validation gap relative to an unconstrained model despite training R^2 remaining higher than validation R^2. Gumara's higher QRF Validation R^2 (0.75 vs. 0.73) may stem from its smaller drainage area (1,394 vs. 1664 km^2), which likely reduces sediment source variability and amplifies flow paths, enhancing model predictability. Gilgel Abay's more distributed sediment sources and higher rainfall variability (Section 4.3) may increase modeling complexity. These findings highlight QRF's suitability for capturing seasonal sediment dynamics (95–96% of yields in the wet season, June–October; Section 3.4), supporting its selection for sediment management applications in the UBNB.

4.2 Dominance of Discharge-Derived Features

Feature importance analysis from the QRF model (Section 3.2; Figure 7; Table 6) revealed that the two watersheds are governed by different combinations of predictors rather than a single dominant driver common to both. In Gilgel Abay, short-lag rainfall terms (P_lag_1, P_lag_3) and the seasonal cosine term led the ranking, whereas in Gumara, evapotranspiration, temperature, and the 1-day discharge lag carried the greatest weight; the 1-day discharge lag

(Q_lag_1) was nonetheless among the top four predictors in both watersheds, consistent with global studies emphasizing discharge as a dominant control on sediment transport in fluvial systems (Syvitski and Milliman, 2007). The 1-day discharge lag, reflecting near-antecedent flow conditions, highlights short-term temporal dependencies in sediment availability, consistent with studies in the Ethiopian highlands (Easton *et al.*, 2010).

In Gilgel Abay, rainfall-lag terms dominated the ranking (P_lag_1: MDI = 0.15; P_lag_3: 0.12; Table 6), consistent with their comparatively strong SSC correlations (P_lag_1: r = 0.54; P_lag_3: r = 0.49; Table 7), and reflecting this watershed's larger, wetter catchment area (1,664 km^2, ~1,861 mm/yr; Section 2.1). Instantaneous rainfall (P) had a moderate correlation with SSC (r = 0.40; Table 7) but ranked below its own lagged forms in importance, consistent with an indirect, delayed influence via runoff generation rather than a direct same-day effect. In Gumara, by contrast, ETo and temperature ranked highest (MDI = 0.15 and 0.13, respectively; Table 6), both carrying negative correlations with SSC (ETo: r = -0.45; T: r = -0.14; Table 7), consistent with reduced evaporative demand coinciding with wetter, higher-sediment conditions. Seasonal terms (Cos_J: MDI = 0.13 for Gilgel Abay, 0.05 for Gumara) further enhanced model sensitivity to monsoon timing. These results indicate that Gilgel Abay's sediment response is more directly rainfall-paced, while Gumara's is more strongly modulated by discharge and atmospheric-demand variables, contrasting with discharge-dominated systems more typically reported elsewhere (Kisi *et al.*, 2024).

4.3 Watershed Specific Differences

Differences in feature importance and predictor–SSC relationships between watersheds highlight the need for tailored, watershed-specific modeling. Gumara’s stronger 1-day discharge-lag correlation with SSC (Q_lag_1: r = 0.41 vs. 0.38 for Gilgel Abay; Table 7) and the dominance of ETo and temperature in its feature-importance ranking (Table 6) are consistent with its steeper topography and more concentrated flow paths, amplifying discharge’s role (Tebebu *et al.*, 2010). Conversely, Gilgel Abay’s stronger short-lag rainfall correlations (P_lag_1: r = 0.54 vs. 0.25 for Gumara; Table 7) and their leading position in its feature-importance ranking (Table 6) point to a more rainfall-paced sediment response, reflecting greater rainfall-driven runoff generation tied to its higher annual rainfall (1,861 vs. 1,403 mm; Section 2.1; (Zeleke et al., 2013; Ayele et al., 2016)). Correlation analysis further reveals inter-watershed variability in the seasonal signal: the cosine Julian-day term is more strongly (negatively) correlated with SSC in Gilgel Abay (Cos_J: r = -0.46) than in Gumara (r

= -0.37; Table 7), while ETo shows the reverse pattern (r = -0.33 for Gilgel Abay vs. -0.45 for Gumara; Table 7), indicating that Gumara's sediment regime is comparatively more sensitive to atmospheric-demand fluctuations. These findings, supported by the predictor–SSC correlations in Table 7 and the feature-importance rankings in Table 6, highlight the importance of watershed-specific models to capture local hydro-geomorphic controls (Nyssen *et al.*, 2004). These watershed-specific differences in sediment-discharge coupling echo broader evidence that seasonal hydrological variability itself reshapes sediment-transport regimes across diverse climatic settings, not only in monsoon basins but also in cryosphere-fed systems undergoing comparable shifts in flow seasonality (Zhang *et al.*, 2023).

4.4 Sediment Yield Validation and Management Implications

Our QRF model estimates net sediment yields of 30.7 ± 7.2 t/ha/yr for Gilgel Abay and 27.5 ± 10.74 t/ha/yr for Gumara (1990–2020), with 95% and 96% occurring in the wet season (Sections 3.3, 3.4). These align with regional studies, though estimates vary due to methods and data periods. Zimale et al. (2018) reported higher yields of 35 t/ha/yr for Gilgel Abay and 49 t/ha/yr for Gumara in the gauged area, using modeling of the available SSC data for a short period (1994–2000), likely capturing peak events. Bogale et al. (2023) reported a sediment yield of 18.9 t/ha/yr for Gumara using field data and geo-morphometric analysis, slightly lower but aligning with our results. Lemma et al. (2019) estimated 22.6 t/ha/yr for Gilgel Abay, including 0.6 t/ha/yr bedload with two years of observed data, which supports our suspended sediment results. Gashaw et al. (2020) estimated 32.8 t/ha/yr gross soil loss for Gilgel Abay using RUSLE, slightly higher due to unaccounted deposition. Gashaw et al. (2021) derived 19.7 t/ha/yr for Gumara with SWAT, reinforced by Best Management Practices (BMPs), slightly lower but consistent. High yields, driven primarily by short-lag rainfall in Gilgel Abay and by discharge and evaporative-demand variables in Gumara (Section 4.2, Table 6), occur alongside observed land-use changes such as urban expansion and cropland intensification (Section 3.5). These LULC associations cannot be interpreted causally, however: both urbanization and the modeled sediment-yield trend could independently reflect a shared driver, such as a regional shift in rainfall intensity or discharge regime over 2000–2020 (Bronstert *et al.*, 2002, 2023), rather than one causing the other. Incorporating LULC variables directly into the predictive model or pursuing scenario-based attribution remains a priority for future work (Section 4.5). The QRF model's robustness, capturing monsoon dynamics (peak discharges of 618.9 m^3/s for Gilgel Abay, 496.3 m^3/s for Gumara; Section 3.4), supports its use for erosion management. The Green Legacy Initiative (GLI, launched in 2019) promotes reforestation and wetland restoration (e.g., papyrus planting at Lake Tana inflows) to trap sediments and reduce runoff, mitigating flooding linked to urban expansion ($r = 0.84$, $p < 0.0001$; Section 3.5). Best Management Practices, like terracing, enhance soil stability (Hurni *et al.*, 2005), reducing sediment loads to the GERD.

4.5 Implications, Limitations, and Future Directions

The QRF model's high predictive accuracy provides actionable insights for sediment management in the UBNB, critical for protecting Lake Tana and the GERD. In Gumara, rising sediment yields driven by intense rainfall highlight the need for enhanced soil conservation, such as reforestation and urban runoff mitigation. Gilgel Abay's yields, influenced by high peak discharge (618.9 m^3/s, specific discharge 0.0037 $m^3/s/ha$) and 940% urban expansion (7.3 to 76 km^2, $r = 0.39$, $p = 0.08$; Table 8, Figure 13), suggest additional factors like rainfall variability (1861 mm/yr) or soil management practices warrant further study. QRF's uncertainty quantification and scalability enhance its potential for region-wide sediment modeling, supporting sustainable management strategies (Francke *et al.*, 2008).

Despite these strengths, limitations constrain QRF's applicability. The limited datasets (251/245 SSC measurements for Gilgel Abay/Gumara) may restrict model generalization, particularly for rare high-magnitude events; expanding datasets with longer time series or additional watersheds could improve robustness. Excluding LULC and soil data limits insights into anthropogenic impacts; significant in the Ethiopian highlands; incorporating these via remote-sensing –using GLAD's Landsat-based LULC maps (e.g., for urbanization, wetland loss) as time-varying predictors in QRF, complemented by higher-resolution Sentinel-2 imagery (10–20 m) for refined classification and Sentinel-1/SMAP data for soil moisture and erodibility mapping–could quantify human induced sediment dynamics such as urban driven runoff ($r = 0.84$ in Gumara) as shown in regional studies (Haregeweyn *et al.*, 2015; Gashaw *et al.*, 2018; Lemma *et al.*, 2019). The QRF model's computational complexity poses challenges for operational use in resource-constrained settings; consequently, exploring hybrid models combining QRF with physically based approaches could balance predictive accuracy and interpretability. The focus on SSC overlooks bedload contributions, which may constitute 10–20% of total sediment in similar systems (Turowski *et al.*, 2010); thus, quantifying bedload through field measurements is essential for a comprehensive sediment budget. Finally, QRF's transferability to other Blue Nile tributaries remains untested; hence, assessing its applicability across the basin could support region-wide sediment management strategies. Relatedly, recurrent sequence models such as Long Short-Term Memory (LSTM) networks were not implemented in this study (Section 2.3.2) but represent a promising direction for future work, given their capacity to learn lag structure directly from the data rather than through pre-specified lag terms; a properly tuned LSTM, benchmarked against the QRF configuration reported here, would be a natural next step. These findings and limitations highlight the need for integrated erosion control (e.g., GLI's reforestation) and advanced modeling to mitigate sedimentation risks to the GERD and ensure sustainable UBNB management.

5. CONCLUSIONS

This study demonstrates that QRF successfully reconstructed sedigraphs for the Gilgel Abay and Gumara watersheds (1990–2020), identifying watershed-specific drivers of sediment dynamics: short-lag rainfall in Gilgel Abay, and discharge and evaporative-demand variables in Gumara. These insights highlight QRF's ability to address data scarcity and non-linear monsoon-driven processes, providing sediment yield estimates with quantified uncertainty that are critical for mitigating erosion risks for Lake Tana and the GERD. The observed co-occurrence of elevated sediment yields with land-use changes such as urban expansion and wetland loss suggests, but does not establish, a land-use influence on sediment dynamics; targeted strategies such as reforestation and urban runoff management remain reasonable precautionary measures for sustainable sediment control regardless of the precise causal pathway. Future research should incorporate LULC variables directly into the predictive framework or pursue scenario-based attribution to resolve this uncertainty, alongside integrating GLAD-derived land-use and remote-sensing-based soil data (e.g., Sentinel-2 and Sentinel-1 as SSC predictors), expanding datasets across UBNB watersheds, quantifying bedload, developing hybrid models, and testing QRF's regional transferability to enhance resilience against climate and anthropogenic pressures.

ACKNOWLEDGEMENTS

We thank the Ethiopian Meteorological Institute (EMI) for rainfall and temperature data, the Ministry of Water and Energy (MoWE) and Abay Basin Authority (ABAO) for discharge and suspended sediment concentration data, and the University of Maryland for the GLAD land-use dataset. We also thank the Bahir Dar Institute of Technology, the Bahir Dar University, and the Institute of Environmental Sciences and Geography, University of Potsdam, Campus Golm, for academic and institutional support. This research is part of the SPS-Blue Nile Project

(Development and Transfer of a Seamless Prediction System for Decision Support in Transboundary Water Management of the Blue Nile), funded by the German Federal Ministry of Education and Research (BMBF) under the Water as a Global Resource (GRoW) program (Grant No. 02WGR1643A-C).

DATA AVAILABILITY

Due to institutional restrictions, the datasets used in this study cannot be publicly shared. Access will be granted by the corresponding author upon reasonable request.

REFERENCES

Abtew W, Dessu SB. 2019. *The grand Ethiopian renaissance dam on the Blue Nile*. Springer.

AlDahoul N, Ahmed AN, Allawi MF, Sherif M, Sefelnasr A, Chau K, El-Shafie A. 2022. A comparison of machine learning models for suspended sediment load classification. *Engineering Applications of Computational Fluid Mechanics* **16** (1): 1211–1232

Almubaidin MAA, Latif SD, Balan K, Ahmed AN, El-Shafie A. 2023. Enhancing sediment transport predictions through machine learning-based multi-scenario regression models. *Results in Engineering* **20**: 101585

Annys S, Adgo E, Ghebreyohannes T, Van Passel S, Dessein J, Nyssen J. 2019. Impacts of the hydropower-controlled Tana-Beles interbasin water transfer on downstream rural livelihoods (northwest Ethiopia). *Journal of Hydrology* **569**: 436–448

Ariano SS, Ali G. 2024. Hydrometric data discretization into environmental flow components: a new, practical approach to explore concentration-discharge relationships. *Canadian Water Resources Journal/Revue canadienne des ressources hydriques* **49** (4): 441–459

Asselman NEM. 2000. Fitting and interpretation of sediment rating curves. *Journal of Hydrology* **234** (3–4): 228–248

Ayele HS, Li M-H, Tung C-P. 2016. Assessing climate change impact on Gilgel Abbay and Gumara watershed hydrology, the upper Blue Nile basin, Ethiopia. *Terrestrial, Atmospheric & Oceanic Sciences* **27** (6)

Bezak N, Lebar K, Bai Y, Rusjan S. 2025. Using Machine Learning to Predict Suspended Sediment Transport under Climate Change: Using Machine Learning to Predict Suspended Sediment Transport under Climate Change. *Water Resources Management* **39** (7): 3311–3326

Bihonegn BG, Awoke AG. 2025. Spatiotemporal sediment yield variability in the Upper Blue Nile Basin, Ethiopia. *Earth Science Informatics* **18** (3): 319

Bogale AG, Anwar A. A, Wolde M, and Steenhuis TS. 2023. Application of geomorphometric characteristics to prioritize watersheds for soil and water conservation practices in the Lake Tana Basin, Ethiopia. *Geocarto International* **38** (1): 2184502 DOI: 10.1080/10106049.2023.2184502

Bronstert A, Niehoff D, Bürger G. 2002. Effects of climate and land-use change on storm runoff generation: present knowledge and modelling capabilities. *Hydrological processes* **16** (2): 509–529

Bronstert A, Niehoff D, Schiffler GR. 2023. Modelling infiltration and infiltration excess: The importance of fast and local processes. *Hydrological Processes* **37** (4): e14875

Carrivick JL, Tweed FS. 2021. Deglaciation controls on sediment yield: Towards capturing spatio-temporal variability. *Earth-Science Reviews* **221**: 103809

Conway D. 2000. The climate and hydrology of the Upper Blue Nile River. *The Geographical Journal* **166** (1): 49–62 DOI: https://doi.org/10.1111/j.1475-4959.2000.tb00006.x

Deng W, Guo Y, Liu J, Li Y, Liu D, Zhu L. 2019. A missing power data filling method based on improved random forest algorithm. *Chinese Journal of Electrical Engineering* **5** (4): 33–39

Dessie M, Verhoest N, Pauwels V, Poesen J, Adgo E, Deckers S, Nyssen J. 2015. Runoff delivery from the hilly catchments of Lake Tana basin. *Tropical lakes in a changing environment: water, land, biology, climate and humans. International ConferenceTropilakes 2015. Bahir Dar University, Bahir Dar, Ethiopia, Preconference excursion guide*: 3–6

Easton ZM, Fuka DR, Walter MT, Cowan DM, Schneiderman EM, Steenhuis TS. 2010. Re-conceptualizing the soil and water assessment tool (SWAT) model for a sediment-laden river. *Journal of Hydrology* **389** (3–4): 364–375 DOI: https://doi.org/10.1016/j.jhydrol.2010.06.017

Elsanabary MH, Gan TY. 2015. Evaluation of climate anomalies impacts on the Upper Blue Nile Basin in Ethiopia using a distributed and a lumped hydrologic model. *Journal of Hydrology* **530**: 225–240

Engida AN. 2010. Hydrological and suspended sediment modeling in the Lake Tana Basin, Ethiopia

Enku T, Melesse AM. 2014. A simple temperature method for the estimation of evapotranspiration. *Hydrological Processes* **28** (6): 2945–2960

Fenta AA, Yasuda H, Shimizu K, Haregeweyn N. 2017. Response of streamflow to climate variability and changes in human activities in the semiarid highlands of northern Ethiopia. *Regional Environmental Change* **17** (4): 1229–1240 DOI: 10.1007/s10113-017-1103-y

Francke T, López-Tarazón JA, Schröder B. 2008. Estimation of suspended sediment concentration and yield using linear models, random forests and quantile regression forests. *Hydrological Processes: An International Journal* **22** (25): 4892–4904

Gashaw T, Dile YT, Worqlul AW, Bantider A, Zeleke G, Bewket W, Alamirew T. 2021. Evaluating the effectiveness of best management practices on soil erosion reduction using the SWAT Model: for the case of Gumara watershed, Abbay (Upper Blue Nile) Basin. *Environmental Management* **68** (2): 240–261

Gashaw T, Tulu T, Argaw M, Worqlul AW, Tolessa T, Kindu M. 2018. Estimating the impacts of land use/land cover changes on Ecosystem Service Values: The case of the Andassa watershed in the Upper Blue Nile basin of Ethiopia. *Ecosystem Services* **31**: 219–228

Gashaw T, Worqlul AW, Dile YT, Addisu S, Bantider A, Zeleke G. 2020. Evaluating potential impacts of land management practices on soil erosion in the Gilgel Abay watershed, upper Blue Nile basin. *Heliyon* **6** (8): e04777 DOI: 10.1016/j.heliyon.2020.e04777

Guzman CD, Tilahun SA, Zegeye AD, Steenhuis TS. 2013. Suspended sediment concentration–discharge relationships in the (sub-) humid Ethiopian highlands. *Hydrology and Earth System Sciences* **17** (3): 1067–1077

Hansen MC, Potapov P V, Moore R, Hancher M, Turubanova SA, Tyukavina A, Thau D, Stehman S V, Goetz SJ, Loveland TR. 2013. High-resolution global maps of 21st-century forest cover change. *science* **342** (6160): 850–853

Haregeweyn N, Poesen J, Nyssen J, Verstraeten G, de Vente J, Govers G, Moeyersons J. 2015. Soil erosion and conservation in Ethiopia: A review. *Progress in Physical Geography* **39** (6): 750–774

Haregeweyn N, Tsunekawa A, Poesen J, Tsubo M, Meshesha DT, Fenta AA, Nyssen J, Adgo E. 2017. Comprehensive assessment of soil erosion risk for better land use planning in river basins: Case study of the Upper Blue Nile River. *Science of the Total Environment* **574** DOI: 10.1016/j.scitotenv.2016.09.019

Horowitz AJ. 2003. An evaluation of sediment rating curves for estimating suspended sediment concentrations for subsequent flux calculations. *Hydrological Processes* **17** (17): 3387–3409 DOI: https://doi.org/10.1002/hyp.1299

Hunter JD. 2007. Matplotlib: A 2D graphics environment. *Computing in science & engineering* **9** (03): 90–95

Hurni H, Tato K, Zeleke G. 2005. The implications of changes in population, land use, and land management for surface runoff in the upper Nile basin area of Ethiopia. *Mountain research and development* **25** (2): 147–154

Jarri SA. 2024. Urban Energy Modelling: An Integration of Data-Driven, Machine Learning and Deep Learning Techniques

Kar R, Sarkar A. 2022. Impact of anthropocene on the fluvial sediment supply: The mahanadi river basin perspective. In *River Dynamics and Flood Hazards: Studies on Risk and Mitigation*Springer; 241–282.

Kisi O, Heddam S, Parmar KS, Yaseen ZM, Kulls C. 2024. Improved monthly streamflow prediction using integrated multivariate adaptive regression spline with K-means clustering: implementation of reanalyzed remote sensing data. *Stochastic Environmental Research and Risk Assessment* **38** (6): 2489–2519

Kumlachew YZ, Tilahun SA, Cherie FF, Akale AT, Kibret EA, Alemie NA, Animut M. 2023. Quantifying flow rate using stage-discharge rating curve and Scs runoff equation on upland watershed of Lake Tana Sub Basin, Ethiopia. *Sustainable Water Resources Management* **9** (2): 47

Lemma H, Frankl A, van Griensven A, Poesen J, Adgo E, Nyssen J. 2019. Identifying erosion hotspots in Lake Tana Basin from a multisite Soil and Water Assessment Tool validation: Opportunity for land managers. *Land Degradation & Development* **30** (12): 1449–1467

Lund JW, Groten JT, Karwan DL, Babcock C. 2022. Using machine learning to improve predictions and provide insight into fluvial sediment transport. *Hydrological Processes* **36** (8): e14648

Meinshausen N. 2006. Quantile regression forests. *Journal of Machine Learning Research* **7**: 983–999

Meinshausen N, Ridgeway G. 2006. Quantile regression forests. *Journal of machine learning research* **7** (6)

Nearing GS, Kratzert F, Sampson AK, Pelissier CS, Klotz D, Frame JM, Prieto C, Gupta H V. 2021. What role does hydrological science play in the age of machine learning? *Water Resources Research* **57** (3): e2020WR028091

Negatu TA, Zimale FA, Steenhuis TS. 2022. Establishing stage-discharge rating curves in developing countries: Lake Tana basin, Ethiopia. Hydrology 2022, 9, 13

Nourani V, Molajou A, Tajbakhsh AD, Najafi H. 2019. A wavelet based data mining technique for suspended sediment load modeling. *Water Resources Management* **33**: 1769–1784

Nyssen J, Veyret-Picot M, Poesen J, Moeyersons J, Haile M, Deckers J, Govers G. 2004. The effectiveness of loose rock check dams for gully control in Tigray, northern Ethiopia. *Soil Use and Management* **20** (1): 55–64

Panigrahi N. 2021. Inverse distance weight. In *Encyclopedia of Mathematical Geosciences*Springer; 1–7.

Pedregosa F, Varoquaux G, Gramfort A, Michel V, Thirion B, Grisel O, Blondel M, Prettenhofer P, Weiss R, Dubourg V. 2011. Scikit-learn: Machine learning in Python. *the Journal of Machine Learning Research* **12**: 2825–2830

Potapov P, Hansen MC, Pickens A, Hernandez-Serna A, Tyukavina A, Turubanova S, Zalles V, Li X, Khan A, Stolle F. 2022. The global 2000-2020 land cover and land use change dataset derived from the Landsat archive: first results. *Frontiers in Remote Sensing* **3**: 856903

Schmidt L, Francke T, Mueller EN. 2023. Advances in sediment load prediction using quantile regression forests. *Hydrology and Earth System Sciences* **27** (4): 891–905 DOI: https://doi.org/10.5194/hess-27-891-2023

Syvitski JPM, Milliman JD. 2007. Geology, geography, and humans battle for dominance over the delivery of fluvial sediment to the coastal ocean. *Journal of Geology* **115** (1): 1–19

Syvitski JPM, Vörösmarty CJ, Kettner AJ, Green P. 2005. Impact of humans on the flux of terrestrial sediment to the global coastal ocean. *science* **308** (5720): 376–380

Tebebu TY, Abidoye AB, Steenhuis TS. 2010. Soil erosion and sediment yield in the Upper Blue Nile Basin: A review. *Journal of Environmental Management* **91** (5): 963–971 DOI: https://doi.org/10.1016/j.jenvman.2009.11.006

Teshome A, Demissie TD. 2022. State of Climate in Ethiopia 2021

Turowski JM, Rickenmann D, Dadson SJ. 2010. The partitioning of the total sediment load of a river into suspended load and bedload: a review of empirical data. *Sedimentology* **57** (4): 1126–1146

Virtanen P, Gommers R, Oliphant TE, Haberland M, Reddy T, Cournapeau D, Burovski E, Peterson P, Weckesser W, Bright J. 2020. SciPy 1.0: fundamental algorithms for scientific computing in Python. *Nature methods* **17** (3): 261–272

Walling DE, Fang D. 2003. Recent trends in the suspended sediment loads of the world’s rivers. *Global and planetary change* **39** (1–2): 111–126

Worku KB, Bronstert A, Francke T, Zimale FA. 2026. Combining Machine Learning and Process-Based Modelling for Sediment Load Estimation in the Data-Scarce Kessie Watershed , Upper Blue Nile Basin: 1–30

Worku KB, Sultan D, Haregeweyn N, Berihun ML, Nigatu MB, Aynalem MD. 2025. Hydrological Impact of Khat Cultivation in Aba Gerima Watershed, Lake Tana Basin, Ethiopia. In *Sustainable Development Research in Manufacturing, Process Engineering, Green Infrastructure, and Water Resources: Advancement of Science and Technology*Springer; 395–412.

Zegeye AD, Langendoen EJ, Stoof CR, Tilahun SA, Dagnew DC, Zimale FA, Guzman CD, Yitaferu B, Steenhuis TS. 2016. Morphological dynamics of gully systems in the subhumid Ethiopian Highlands: the Debre Mawi watershed. *Soil* **2** (3): 443–458

Zeleke G, Winterwerp JC, Kelderman P. 2013. Sedimentation and sediment handling in the Blue Nile River system. *Hydrology and Earth System Sciences Discussions* **10** (5): 6457–6492

Zhang T, Li D, East AE, Kettner AJ, Best J, Ni J, Lu X. 2023. Shifted sediment-transport regimes by climate change and amplified hydrological variability in cryosphere-fed rivers. *Science Advances* **9** (45): eadi5019

Zhang T, Li D, East AE, Walling DE, Lane S, Overeem I, Beylich AA, Koppes M, Lu X. 2022a. Warming-driven erosion and sediment transport in cold regions. *Nature Reviews Earth & Environment* **3** (12): 832–851

Zhang T, Li D, Kettner AJ, Zhou Y, Lu X. 2021. Constraining dynamic sediment-discharge relationships in cold environments: The sediment-availability-transport (SAT) model. *Water Resources Research* **57** (10): e2021WR030690

Zhang W, Gu X, Tang L, Yin Y, Liu D, Zhang Y. 2022b. Application of machine learning, deep learning and optimization algorithms in geoengineering and geoscience: Comprehensive review and future challenge. *Gondwana Research* **109**: 1–17

Zhu R, Yang L, Liu T, Wen X, Zhang L, Chang Y. 2019. Hydrological responses to the future climate change in a data scarce region, northwest China: Application of machine learning models. *Water* **11** (8): 1588

Zimale FA, Moges MA, Alemu ML, Ayana EK, Demissie SS, Tilahun SA, Steenhuis TS. 2018. Budgeting suspended sediment fluxes in tropical monsoonal watersheds with limited data: The Lake Tana basin. *Journal of Hydrology and Hydromechanics* **66** (1): 65–78

951